Design and Analysis of Composite Multilayered Shells

Final Technical Report

NSF Award No. DMI-9321005

Ricardo L. Actis, Principal Investigator

October 27, 1997

1.0 Introduction

The principal objective of this investigation was to provide a reliable and efficient prototype software for the engineering design and analysis of multilayered composite shells, capable of modeling linear and nonlinear behavior in three dimensions. In addition, it should be capable of assessing the quality of the solution and providing feedback on the basis of which the solution quality can be improved. Its hierarchic structure should allow the selection of models of increasing complexity in an adaptive way, such that the goals of computation are satisfied within the required accuracy and with minimal effort.

The project addressed the investigation of a hierarchic sequence of models for multilayered composite shells and their implementation within the framework of the p-version of the finite element method. In the Phase I project, we investigated the use of the hierarchic models for the analysis of bending of laminated (flat) plates. Phase II utilized the results of Phase I to fully assess the problems associated with bending/membrane coupling and curvature, and extend those results to the nonlinear (small-strain, large-deformation) solution methods for laminated shells, where the most significant technological contributions are to be realized. The specific objectives addressed in this investigation were:

• Investigation of the problems associated with the implementation of a hierarchic sequence of models for laminated shells within the framework of the p-version of the finite element method as an extension of the work done during the Phase I project for laminated plates.

• Investigation of the added complexity for incorporating coupling between membrane and bending terms, caused by non-symmetric stacking sequences, curvature, etc., and the numerical generation and orthogonalization of the transverse shape functions for shells as an integral part of the solution process.

19990304 063

• Investigation of the use of the *error estimators* proposed during the Phase I research, and the *alternating projection method* as possible adaptive strategies for the automatic selection of models from the hierarchy for a particular application.

• Based on the experience acquired with the design of the prototype software during Phase I research, enhance the prototype software for shells to assess the effectiveness of the hierarchic models to solve computationally intensive problems.

The following objectives were achieved during the Phase II research project:

Task 1: Investigation of the implementation issues of the first model for shells into a prototype software. The significance of this activity was that it allowed addressing the finite element implementation issues early in the project and make the necessary adjustments in a simpler setting. Additionally, we were in a position to address the problems of locking of shells and evaluate mesh designs which were also very important sub-topic of the investigation.

Task 2: The model selection, model construction, and generation of transverse shape functions for higher order models were investigated. This included the basic work leading to adopt the proper strategy for model selection, for the automatic generation of transverse shape functions and for the adaptivity criteria.

Task 3: Incorporation into the prototype software of the additional models and logic for model selection. The additional models can be manually or automatically selected from the available set.

Task 4: Debugging and testing of the prototype software, and solution of benchmark problems, to demonstrate the unique capabilities of the hierarchic models.

2.0 The first shell model

In the first task of the project we addressed the following issues:

- The implementation of the *first hierarchic model*.
- The surface description of the shell and the corresponding *mapping* techniques.
- The formulation to account for *nonlinearities*.

These points are discussed in detail in the following.

2.1 The first hierarchic model

As discussed in our Phase II proposal, the first hierarchic shell model is a five-field semi-discretization which approximates the solution corresponding to the three-dimensional problem with the minimum number of fields.

We consider a curved shell element with arbitrary geometry located in the *xyz* Cartesian coordinate space. Let *r, s, w* denote curvilinear coordinates such that $w = 0$ represents the middle surface of the shell (Figure 1). The shell under consideration is composed of a finite number of orthotropic layers of constant thickness. The thickness of each layer is denoted by h_i, and the total thickness of the shell is $h = \sum_{j=1}^{N} h_i$, where N is the total number of layers. We consider a displacement field which approximates the curvilinear components of the displacement vector. Specifically, the first member of the hierarchic sequence of models is:

$$u_r(r, s, w) = u|_0^r(r, s) + u|_1^r(r, s)w$$

$$u_s(r, s, w) = u|_0^s(r, s) + u|_1^s(r, s)w \tag{1}$$

$$u_w(r, s, w) = u|_0^w(r, s)$$

where (r, s) are the curvilinear coordinates of the middle surface of the shell, and w is the direction of the normal to the middle surface. Figure 1 shows a typical quadrilateral shell element in three-dimensional space (Ω_k) and the corresponding standard quadrilateral element (Ω_{st}).
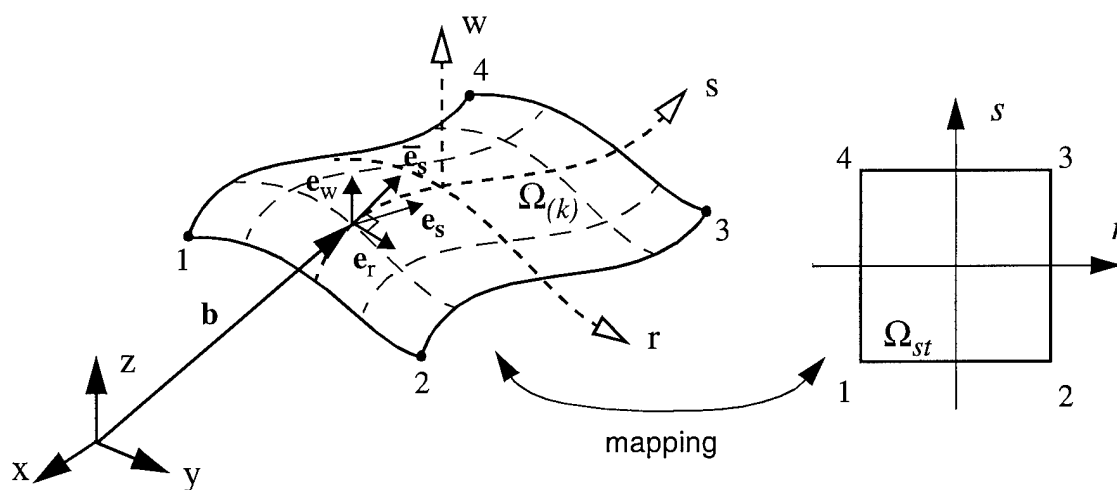

FIGURE 1. Curvilinear coordinates associated with the middle surface of the shell.

The main advantage in approximating the displacement components in the curvilinear system is that each field can be augmented independently for the higher-order models. Also, given the variation in the material properties through the thickness in the case of laminated composites, this makes it possible to utilize a unique set of transverse shape functions per field as discussed in Section 4A of the Phase II proposal. The other advantage is related to the specification of the boundary conditions

(loads and constraints). Working with the natural coordinates of the shell surface simplifies the implementation of traditional constraints, such as simple support, clamped, symmetry, antisymmetry, etc., and the specification of distributed surface or edge tractions, as well as concentrated forces.

One added complexity in working with the curvilinear coordinates is the incorporation of the rotation matrix into the formulation. The rotation matrix $[R]$ is needed to express the relation between the global (xyz) and curvilinear (rsw) displacement components,

$$\{u\}_{(xyz)} = [R]\{u\}_{(rsw)} \tag{2}$$

and its terms are the components of the normalized covariant basis vectors ($\mathbf{e}_r$, $\mathbf{e}_s$, $\mathbf{e}_w$ in Figure 1) which are computed from the derivatives of the mapping functions. Introducing the following simplified notation to indicate the difference between global and curvilinear components of the displacements: $u_{(xyz)} = u$, $u_{(rsw)} = \underset{\sim}{u}$, Eq. (2) can be rewritten as:

$$\{u\} = [R]\{\underset{\sim}{u}\} \tag{3}$$

The shell middle surface can be written in parametric form as:

$$x = x_0(r,s), \qquad y = y_0(r,s), \qquad z = z_0(r,s) \tag{4}$$

where x_0, y_0, z_0 are smooth mapping function. Therefore considering the position vector $\mathbf{b}$ shown in Figure 1, the normalized covariant basis vectors are defined as:

$$\mathbf{e}_r = \left(\frac{\partial \mathbf{b}}{\partial r} \middle/ \left|\frac{\partial \mathbf{b}}{\partial r}\right|\right), \qquad \mathbf{e}_s = \left(\frac{\partial \mathbf{b}}{\partial s} \middle/ \left|\frac{\partial \mathbf{b}}{\partial s}\right|\right), \qquad \mathbf{e}_w = \mathbf{e}_r \times \mathbf{e}_s \tag{5}$$

with

$$\frac{\partial \mathbf{b}}{\partial r} = \frac{\partial x_0}{\partial r}\vec{i} + \frac{\partial y_0}{\partial r}\vec{j} + \frac{\partial z_0}{\partial r}\vec{k}, \qquad \frac{\partial \mathbf{b}}{\partial s} = \frac{\partial x_0}{\partial s}\vec{i} + \frac{\partial y_0}{\partial s}\vec{j} + \frac{\partial z_0}{\partial s}\vec{k} \tag{6}$$

In Eq. (6), $\vec{i}$, $\vec{j}$, $\vec{k}$ denote the unit vector components in the global coordinate system. The rotation matrix in Eq. (3) is obtained from the Cartesian components of the unit vectors in Eq. (5) as:

$$[R] = \begin{bmatrix} R_1 & R_4 & R_7 \\ R_2 & R_5 & R_8 \\ R_3 & R_6 & R_9 \end{bmatrix} = \begin{bmatrix} e_{rx} & e_{sx} & e_{wx} \\ e_{ry} & e_{sy} & e_{wy} \\ e_{rz} & e_{sz} & e_{wz} \end{bmatrix} \tag{7}$$

Note that the rotation matrix is a function of the curvilinear components (r, s) only. The relevance of the presence of the rotation matrix in the formulation becomes apparent when considering the bilinear form in the expression of the principle of virtual work. Considering the case of no body forces, no spring boundary conditions and homogeneous constraints, the principle of virtual work can be stated as follows (Ref. [1]):

"Find $\{u\} \in S^o$ such that $B(u,v) = F(v)$, for all $\{v\} \in S^o$"

where S^o is the space of admissible functions satisfying the homogeneous boundary conditions, $\{v\}$ are the test functions, $F(v)$ is the virtual work of the applied loads, and $B(u,v)$ is the virtual work of the internal stresses:

$$B(u, v) = \int_V ([D]\{v\})^T [Q][D]\{u\} dV$$

$$F(v) = \int_A \{v\}^T \{T\} dA$$

(8)

In Eq. (8), $\{T\}$ is the vector of the applied tractions in the global coordinate system, $[D]$ is a differential operator in terms of the global coordinates and $[Q]$ is the material stiffness matrix. $[D]$ and $[Q]$ are defined as:

$$[D]^T = \begin{bmatrix} \frac{\partial}{\partial x} & 0 & 0 & 0 & \frac{\partial}{\partial z} & \frac{\partial}{\partial y} \\ 0 & \frac{\partial}{\partial y} & 0 & \frac{\partial}{\partial z} & 0 & \frac{\partial}{\partial x} \\ 0 & 0 & \frac{\partial}{\partial z} & \frac{\partial}{\partial y} & \frac{\partial}{\partial x} & 0 \end{bmatrix} \qquad [Q] = \begin{bmatrix} Q_{11} & Q_{12} & Q_{13} & Q_{14} & Q_{15} & Q_{16} \\ & Q_{22} & Q_{23} & Q_{24} & Q_{25} & Q_{26} \\ & & Q_{33} & Q_{34} & Q_{35} & Q_{36} \\ & & \text{(sym)} & Q_{44} & Q_{45} & Q_{46} \\ & & & & Q_{55} & Q_{56} \\ & & & & & Q_{66} \end{bmatrix}$$

(9)

Introducing Eq. (3) into Eq. (8):

$$B(u, v) = \int_V ([D][R]\{\underset{\sim}{v}\})^T [Q][D]([R]\{\underset{\sim}{u}\}) dV$$

$$F(v) = \int_A ([R]\{\underset{\sim}{v}\})^T \{T\} dA$$

(10)

In Eq. (10) the differential operator $[D]$ acts on the rotation matrix which means that the second derivatives of the mapping functions are also needed. The curvilinear components of the displacement vector are approximated by polynomial functions of the form:

$$\{u\} = [\Phi]\{a\}, \qquad \{v\} = [\Phi]\{b\} \tag{11}$$

in which $[\Phi]$ are known functions of (r,s,w) and $\{a\}$, $\{b\}$ are the amplitudes of the basis functions. The basis functions are given as the product of a function of (r, s) times a function of w (see Eq. (1)) as follows:

$$[\Phi] = \begin{bmatrix} 1 & 0 & w & 0 & 0 \\ 0 & 1 & 0 & w & 0 \\ 0 & 0 & 0 & 0 & 1 \end{bmatrix} \phi_i(r,s) \tag{12}$$

where $\phi_i(r,s)$ are the hierarchic basic shape functions characterized by the polynomial degree p and the mapping functions, and are given in Ref. [1]. Substituting Eq. (11) into Eq. (10), the expression of the principle of virtual work can be witten in matrix form:

$$\{b\}^T \left(\int_V ([D][R][\Phi])^T [Q][D][R][\Phi] dV \right) \{a\} = \{b\}^T \int_A ([R][\Phi])^T \{T\} dA \tag{13}$$

which has to be satisfied for any $\{b\}$. Therefore, Eq. (13) can be written in compact form as:

$$[K]\{a\} = \{q\} \tag{14}$$

where $[K]$ is the system stiffness matrix and $\{q\}$ is the load vector. For any element (e) in the mesh, the stiffness matrix and load vector terms are given by:

$$K_{ij}^{(e)} = \int_V ([D][R]\{\Phi\}_i)^T [Q][D][R]\{\Phi\}_j \, dV$$

$$q_i^{(e)} = \int_A ([R]\{\Phi\}_i)^T \{T\} dA \tag{15}$$

where $\{\Phi\}_i$ is a column of the matrix in Eq. (12). The solution of the linear system of equations represented by Eq. (14), are the curvilinear components of the displacement vector.

As mentioned earlier, the coefficients of the rotation matrix $[R]$ are the Cartesian components of the normalized covariant basis vectors $\{e_r \, e_s \, e_w\}^T$ which are computed from the derivatives of the map-

ping functions of the shell middle surface. In general, the components of the normalized covariant basis vectors (e_r, e_s) are non-orthogonal. In our first implementation of this model the non-orthogonal basis was used. After a few model problems were solved using the prototype software, it became apparent that the computation of the material matrix with respect to a non-orthogonal basis would impose additional complications, and a change was required. An orthogonal basis was developed to overcome this difficulty. The orthogonalization was performed by recomputing the unit vector in one direction on the shell surface as the cross product of the vector normal to the surface (e_w) and the other unit vector on the surface (e_r): $\bar{e}_s = e_w \times e_r$ (see Figure 1). With this change, the computation of the material stiffness matrix was simplified for both homogeneous and laminated shells.

The material stiffness matrix $[Q]$ needed to compute the element stiffness matrix in Eq. (15) is determined as follows: Let w (the shell thickness direction) be the direction of the layup of the laminae. The material properties of each layer are defined in the principal material directions of the lamina $(\bar{x}\ \bar{y}\ \bar{z})$. Let the relation between the global and lamina coordinate systems at a point within the ith lamina be:

$$\left\{ \begin{array}{c} \bar{x} \\ \bar{y} \\ \bar{z} \end{array} \right\}_{(i)} = \begin{bmatrix} l_1 & l_2 & l_3 \\ m_1 & m_2 & m_3 \\ n_1 & n_2 & n_3 \end{bmatrix}_{(i)} \left\{ \begin{array}{c} x \\ y \\ z \end{array} \right\} \tag{16}$$

The stress-strain relation for the ith-lamina in the principal material directions is given by:

$$\left\{ \begin{array}{c} \bar{\sigma}_x \\ \bar{\sigma}_y \\ \bar{\sigma}_z \\ \bar{\tau}_{yz} \\ \bar{\tau}_{zx} \\ \bar{\tau}_{xy} \end{array} \right\}_{(i)} = \begin{bmatrix} C_{11} & C_{12} & C_{13} & 0 & 0 & 0 \\ & C_{22} & C_{23} & 0 & 0 & 0 \\ & & C_{33} & 0 & 0 & 0 \\ & & & C_{44} & 0 & 0 \\ & (\text{sym}) & & & C_{55} & 0 \\ & & & & & C_{66} \end{bmatrix}_{(i)} \left\{ \begin{array}{c} \bar{\varepsilon}_x \\ \bar{\varepsilon}_y \\ \bar{\varepsilon}_z \\ \bar{\gamma}_{yz} \\ \bar{\gamma}_{zx} \\ \bar{\gamma}_{xy} \end{array} \right\}_{(i)}$$

or, in short notation,

$$\{\bar{\sigma}\}_{(i)} = [C]_{(i)}\{\bar{\varepsilon}\}_{(i)} \tag{17}$$

while the same relation in the global coordinate system is:

$$\{\sigma\}_{(i)} = [Q]_{(i)}\{\varepsilon\}_{(i)} \tag{18}$$

For an orthotropic material, the [C] matrix contains 9 independent stiffness coefficients. The relation between the strains in the lamina system and the strains in the global system is given by (Ref. [2]):

$$\left\{ \begin{array}{c} \bar{\varepsilon}_x \\ \bar{\varepsilon}_y \\ \bar{\varepsilon}_z \\ \bar{\gamma}_{yz} \\ \bar{\gamma}_{zx} \\ \bar{\gamma}_{xy} \end{array} \right\}_{(i)} = \begin{bmatrix} l_1^2 & l_2^2 & l_3^2 & l_2 l_3 & l_3 l_1 & l_1 l_2 \\ m_1^2 & m_2^2 & m_3^2 & m_2 m_3 & m_3 m_1 & m_1 m_2 \\ n_1^2 & n_2^2 & n_3^2 & n_2 n_3 & n_3 n_1 & n_1 n_2 \\ 2m_1 n_1 & 2m_2 n_2 & 2m_3 n_3 & m_3 n_2 + m_2 n_3 & m_3 n_1 + m_1 n_3 & m_1 n_2 + m_2 n_1 \\ 2l_1 n_1 & 2l_2 n_2 & 2l_3 n_3 & l_3 n_2 + l_2 n_3 & l_3 n_1 + l_1 n_3 & l_1 n_2 + l_2 n_1 \\ 2l_1 m_1 & 2l_2 m_2 & 2l_3 m_3 & l_3 m_2 + l_2 m_3 & l_3 m_1 + l_1 m_3 & l_1 m_2 + l_2 m_1 \end{bmatrix}_{(i)} \left\{ \begin{array}{c} \varepsilon_x \\ \varepsilon_y \\ \varepsilon_z \\ \gamma_{yz} \\ \gamma_{zx} \\ \gamma_{xy} \end{array} \right\}_{(i)}$$

or, in short notation,

$$\{\bar{\varepsilon}\}_{(i)} = [H]_{(i)}\{\varepsilon\}_{(i)} \tag{19}$$

The strain energy density for the ith-lamina, $U_{(i)}$, is an invariant, and therefore it is the same regardless of the coordinate system:

$$U_{(i)} = \frac{1}{2}\{\sigma\}_{(i)}^T\{\varepsilon\}_{(i)} = \frac{1}{2}\{\bar{\sigma}\}_{(i)}^T\{\bar{\varepsilon}\}_{(i)} \tag{20}$$

Substituting Eqs. (17), (18) and (19) into Eq. (20) we get:

$$U_{(i)} = \frac{1}{2}\{\varepsilon\}_{(i)}^T[Q]_{(i)}\{\varepsilon\}_{(i)} = \frac{1}{2}\{\varepsilon\}_{(i)}^T[H]_{(i)}^T[C]_{(i)}[H]_{(i)}\{\varepsilon\}_{(i)}$$

and therefore, from the above equation, the material stiffness matrix corresponding to the ith-lamina in the global coordinate system is given by:

$$[Q]_{(i)} = [H]_{(i)}^T[C]_{(i)}[H]_{(i)} \tag{21}$$

For each lamina the material matrix is transformed from the material coordinate system to the global coordinate system using Eq. (21). In computing the element stiffness matrix in Eq. (15), the numerical integration is performed layer-by-layer in order to include its material properties.

2.2   Shell mapping

The quality of the mapping procedure has a substantial impact on the quality of the finite element approximation. In the p-version of the finite element method large elements are generally used, and therefore accurate representation of surfaces is essential so that the errors of discretization can be controlled by the mesh and the polynomial order rather than by the mapping of the elements. We have investigated a mapping technique for shells in which the surfaces are approximated by piecewise interpolation polynomials using special collocation points. This method, developed at the University of Maryland , College Park [3], and investigated at Washington University in St. Louis [4], is called *Quasi-Regional Mapping*, and has been implemented in the prototype software for shells.

To demonstrate the quality of mapping obtained by this method, consider the problem shown in Figure 2, which represents the canopy of a jet fighter. The canopy was created by connecting a set of elliptical arcs by a NURBS (Non Uniform Rational B-Spline) surface. Two meshes, one consisting of four quadrilateral shell elements, the other of six elements, were attached to the surface as shown in the figure. Visually, the mapping is able to capture all essential features of the underlying surface. Numerical investigation of the quality of the mapping approximation and its influence in the data extraction from the finite element solution can be found in Ref. [4].

In the case of shells, additional requirements on the quality of the mapping procedures are imposed by the need to approximate the second derivatives well. The second derivatives of the mapping functions are required in the computation of the derivatives of the rotation matrix in Eq. (7) to be used in the computation of the stiffness matrix of the elements. To illustrate this point, consider the product $[D][R]$ in Eq. (15). Given the definitions of $[R]$ and $[D]$ in Eqs. (7) and (9) respectively, the derivative of R_1 with respect to x, for example, will be given as:

$$\frac{\partial R_1}{\partial x} = \frac{\partial R_1}{\partial r}\frac{\partial r}{\partial x} + \frac{\partial R_1}{\partial s}\frac{\partial s}{\partial x}$$

but the derivative of R_1 with respect to the curvilinear coordinates should be further expanded in terms of the mapping functions in Eq. (4) as follows:

$$\frac{\partial R_1}{\partial r} = \frac{\partial e_{rx}}{\partial r} = \frac{E\frac{\partial^2 x_0}{\partial r^2} - \frac{\partial x_0}{\partial r}\left(\frac{\partial x_0}{\partial r}\frac{\partial^2 x_0}{\partial r^2} + \frac{\partial y_0}{\partial r}\frac{\partial^2 y_0}{\partial r^2} + \frac{\partial z_0}{\partial r}\frac{\partial^2 z_0}{\partial r^2}\right)}{E^{3/2}}$$

$$E = \left(\frac{\partial x_0}{\partial r}\right)^2 + \left(\frac{\partial y_0}{\partial r}\right)^2 + \left(\frac{\partial z_0}{\partial r}\right)^2$$

Elliptical arcs

4-element mesh

NURBS surface

6-element mesh
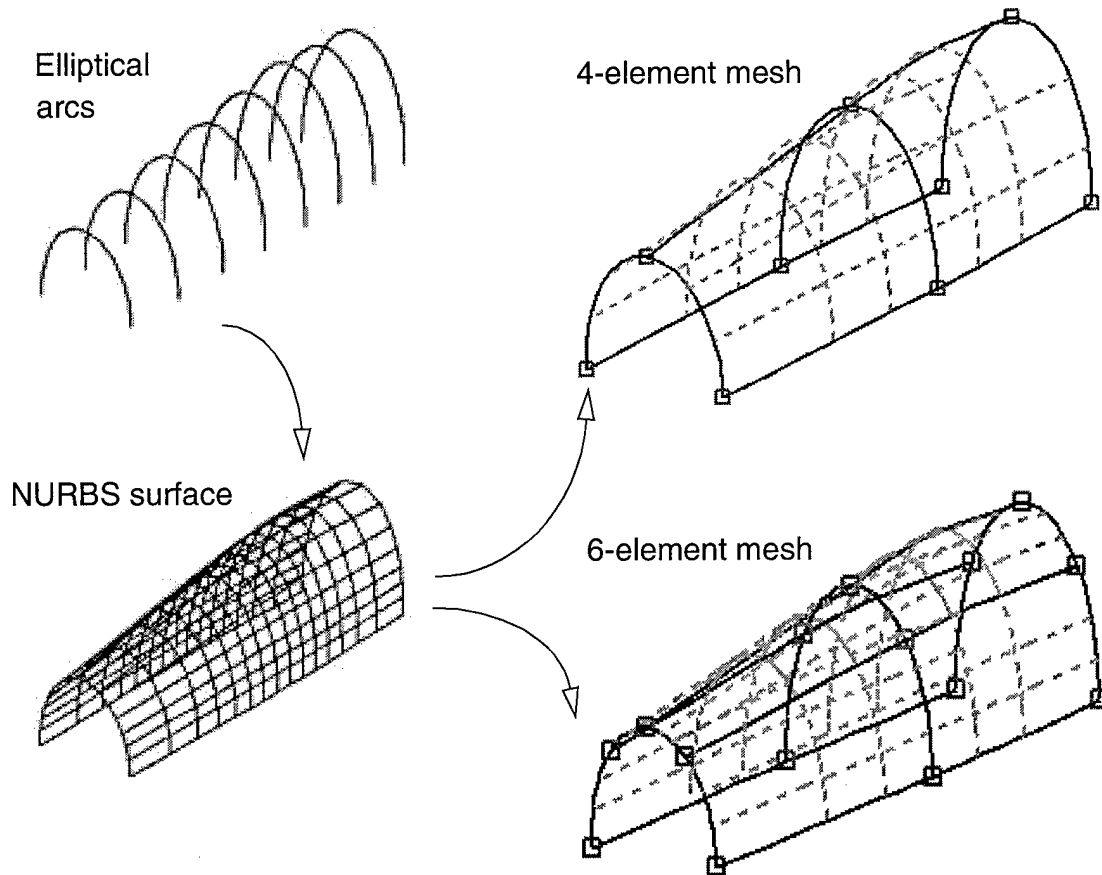
FIGURE 2. Example of *Quasi-Regional* mapping for shells.

and similarly for other terms. The second derivative of the mapping function appears explicitly in the derivative of the rotation matrix components. This clearly indicates that unless smooth mapping functions are used, errors will be introduced in the formulation which are not related to the those introduced by the dimensionally reduced model. These mapping procedures have been implemented and tested in the prototype software.

2.3 Nonlinear formulation

Three types of nonlinearities were considered for the five-field semi-discretization as indicated in the following:

- *Geometric nonlinearities*: Small-strain, large-displacement problems in which the action produced by the loading changes as the body deforms.

- *Eigenvalue buckling*: Determination of the bifurcation buckling loads for shells subjected to arbitrary loading.

- *Pre-stress modal analysis*: Effects of pre-stresses due to arbitrary loading on the natural frequency of vibration of shells.

The eigenvalue buckling and the pre-stress modal analysis are linearized nonlinear problems that can be solved in a two-step operation. The geometric nonlinear problem on the other hand is a fully non-linear problem in which the number of required iterations is problem-dependent.

2.3.1 Geometric nonlinearities

Traditional finite element formulations of geometrically nonlinear problems are based on the Lagrangian description of the equilibrium equations. Several algorithms of this formulation are available in the literature. These include the total Lagrangian, the updated Lagrangian and the 'co-rotational algorithm' for beams and shells (see, for example, Refs. [6]-[7]-[8]).

The discretization procedures for geometrically nonlinear problems has been associated almost exclusively with the h-version of the finite element method. Although the p-version of the finite element method has been addressed in several papers (Refs. [9]-[10]), the formulation is based on the Lagrangian description.

In our work, the geometrically nonlinear problem is formulated using a weak form of the spacial/ Eulerian representation of the equilibrium equations. This approach has the following advantages over the Lagrangian description:

- The equilibrium equations are satisfied in the deformed configuration.

- The displacement components approximated by high-order polynomials and the quasi-regional mapping provide an accurate description of the deformed configuration and makes control of discretization errors possible in practice.

- The simulation of non-conservative loads, such as follower loads, does not require any additional extensions in the formulation, nor does it affect the symmetry of the resulting stiffness matrix.

- The extraction of stresses from the finite element solution is straightforward, since in this approach the equilibrium equations are expressed in terms of the Cauchy stresses.

The spatial/Eulerian formulation of the geometrically nonlinear problem can be summarized as follows (Ref. [5]): The effect of large displacements is accounted for by considering the equilibrium equations in the deformed configuration. The mapping functions are updated using the displacement vector, and the strains and stresses are computed with respect to the deformed configuration (using the Almansi strains and the Cauchy stresses). The resulting nonlinear system is solved by iterative methods. For the particular case of shells, the formulation is described in the following.

Considering the case of no body forces, no spring boundary conditions and homogeneous constraints, the principle of virtual work can be stated as follows:

"Find $\{u\} \in S^{o}$ such that $B(u,v) = F(v)$, for all $\{v\} \in S^{o}$"

where S^o is the space of admissible functions satisfying the homogeneous boundary conditions, $\{u\}$ are the trial functions, $\{v\}$ are the test functions, $F(v)$ is the virtual work of the applied loads, and $B(u,v)$ is the virtual work of the internal stresses:

$$B(u, v) = \int_V \{\varepsilon^{(v)}\}^T [Q]\{\varepsilon^{(u)}\} dV$$

$$F(v) = \int_A \{v\}^T \{T\} dA$$

(22)

which differs from Eq. (8) in that $\{\varepsilon^{(u)}\}$ is the Almansi strain tensor defined in the global coordinate system due to the trial functions and $\{\varepsilon^{(v)}\}$ is the linear strain tensor due to the test functions. That is:

$$\{\varepsilon^{(u)}\} = \{\varepsilon_0^{(u)}\} - \{\Delta\varepsilon^{(u)}\}$$

$$\{\varepsilon^{(v)}\} = \{\varepsilon_0^{(v)}\}$$

(23)

where $\{\varepsilon_0\}$ are the linear components of strain and $\{\Delta\varepsilon\}$ are the nonlinear components as shown below:

$$\varepsilon_{0(ij)}^{(u)} = \frac{1}{2}(u_{i,j} + u_{j,i}) = [D]\{u\}, \qquad \varepsilon_{0(ij)}^{(v)} = \frac{1}{2}(v_{i,j} + v_{j,i}) = [D]\{v\}$$

(24)

$$\Delta\varepsilon_{ij}^{(u)} = \frac{1}{2}u_{k,i}u_{k,j}, \qquad k = 1,2,3$$

where the repeated index indicates summation, and $u_{i,j}$ represents the derivative of u_i with respect to x_j. Note that only the linear definition of strains is considered for the trial function. Substituting Eq. (23) into the bilinear form of Eq. (22), we have:

$$B(u, v) = \int_V \{\varepsilon^{(v)}\}^T [Q]\{\varepsilon_0^{(u)}\} dV - \int_V \{\varepsilon^{(v)}\}^T [Q]\{\Delta\varepsilon^{(u)}\} dV$$

(25)

and considering the relationship between the curvilinear and global components of the displacement vector in Eq. (3) and the strain definition in Eq. (24), we have:

$$B(u, v) = \int_V ([D][R]\{v\})^T [Q][D]([R]\{u\}) dV - \int_V ([D][R]\{v\})^T [Q]\{\Delta\varepsilon^{(u)}\} dV$$

$$F(v) = \int_A ([R]\{v\})^T \{T\} dA$$

(26)

Substituting Eq. (11) into Eq. (26) and rearranging, the principle of virtual work can be written as:

$$\{b\}^T \left(\int_V ([D][R][\Phi])^T [Q][D][R][\Phi] dV \right) \{a\} = \{b\}^T \left(\int_A ([R][\Phi])^T \{T\} dA \right. +$$

$$\left. \int_V ([D][R][\Phi])^T [Q]\{\Delta\varepsilon^{(u)}\} dV \right) \quad (27)$$

which has to be satisfied for any $\{b\}$. Note that the contribution of the nonlinear strains have been moved to the right-hand-side of the equation, as a 'load vector' term. Therefore, Eq. (27) can be written in compact form:

$$[K]\{a\} = \{q\} + \{\Delta q\} \quad (28)$$

where:

$$K_{ij} = \int_V ([D][R]\{\Phi\}_i)^T [Q][D][R]\{\Phi\}_j \, dV$$

$$q_i = \int_A ([R]\{\Phi\}_i)^T \{T\} dA$$

$$\Delta q_i = \int_V ([D][R]\{\Phi\}_i)^T [Q]\{\Delta\varepsilon^{(u)}\} dV$$

Note that Δq_i depends on the solution, and therefore the system can only be solved by an iterative procedure. Denoting the kth-iteration by a superscript (k), Eq. (28) can be witten as:

$$[K^{(k-1)}]\{a^{(k)}\} = \{q^{(k-1)}\} + \{\Delta q^{(k-1)}\} \quad (29)$$

In the computation of the stiffness matrix, load vector and contribution of nonlinear strains in Eq. (29), the mapping updated by the solution corresponding to the $(k-1)$ iteration is used. In other words, during the kth-iteration, the mapping functions are given by:

$$x^{(k)} = x_0(r,s) + u_x^{(k-1)}(r,s,0)$$

$$y^{(k)} = y_0(r,s) + u_y^{(k-1)}(r,s,0) \quad (30)$$

$$z^{(k)} = z_0(r,s) + u_z^{(k-1)}(r,s,0)$$

where the displacements in the global coordinates are computed from the curvilinear displacement at the shell middle surface ($w = 0$) using the rotation matrix corresponding to the (k-1) iteration:

$$\{u^{(k-1)}\} = [R^{(k-1)}]\{\underset{\sim}{u}^{(k-1)}\}$$

This formulation has been implemented in the prototype software for planar and three-dimensional elasticity problems. The results of the preliminary investigation clearly demonstrated the potential of the proposed method for solving geometrically nonlinear problems for shell structures. An example of the implementation is included in the next section.

2.3.2 Eigenvalue buckling

Another class of problems in the analysis of shell structures is eigenvalue buckling which is a linearized form of a geometrically nonlinear formulation, useful for estimating the limits of elastic stability. A capability to perform eigenvalue buckling for homogeneous and laminated shells was developed and implemented. The main points of the formulation are outlined in the following.

The undeformed configuration of the shell is denoted by Ω and its boundary by $\partial\Omega$. The infinitesimal strain is defined in terms of the Cartesian components of the displacements (u_i, i=1, 2, 3):

$$\varepsilon_{ij} = \frac{1}{2}(u_{i,j} + u_{j,i})$$

which is a simplification of the Green-Lagrange strains defined by

$$\Xi_{ij} = \varepsilon_{ij} + \frac{1}{2}(u_{\alpha,i}\ u_{\alpha,j})$$

The simplification is justified by the assumption that $|u_{i,j}| \ll 1$ and hence the product terms $u_{\alpha,i}\ u_{\alpha,j}$ are negligible in relation to $u_{i,j}$. The stress-strain relationship is:

$$\sigma_{ij} = \sigma_{ij}^0 + C_{ijkl}\varepsilon_{kl}$$

where σ_{ij}^0 is a pre-existing stress state, independent of u_i, and C_{ijkl} is the tensor of the elastic moduli of the material. An important property of σ_{ij}^0 is that it is in equilibrium with the corresponding tractions $T_i^0 = \sigma_{ij}^0\ n_j$ in the sense:

$$\frac{1}{2}\int_\Omega \sigma_{ij}^0(v_{i,j} + v_{j,i})dV = \int_{\partial\Omega} T_i^0 v_i dA \qquad for \ all \ v_i \in \overset{\circ}{E}\ (\Omega) \tag{31}$$

where dV and dA represent the differential volume and differential area, respectively, and $\overset{o}{E}$ (Ω) is the space of kinematically admissible perturbations.

When the reference configuration is stress-free (i.e., $\sigma_{ij}^0 = 0$) then the potential energy is defined by:

$$\Pi(u_i) = \frac{1}{2}\int_\Omega C_{ijkl}\varepsilon_{ij}\varepsilon_{kl}dV - \int_{\partial\Omega} T_i u_i dA$$

The exact solution minimizes Π on the set of all kinematically admissible functions denoted by $\tilde{E}(\Omega)$. When the reference configuration is not stress-free then the work done by σ_{ij}^0 due to the non-linear strain terms may not be negligible. Therefore the potential energy expression is written in the following form:

$$\Pi(u_i) = \frac{1}{2}\int_\Omega C_{ijkl}\varepsilon_{ij}\varepsilon_{kl}dV + \frac{1}{2}\int_\Omega \sigma_{ij}^0 u_{\alpha,i} u_{\alpha,j} dV - \int_{\partial\Omega} T_i u_i dA \tag{32}$$

The second integral in Eq. (32) represents the work done by the initial stresses due to the nonlinear strain terms. The work done by σ_{ij}^0 due to the linear strain terms is cancelled by the work done by T_i^0 in the sense of Eq. (31). The discretized form of the potential energy in Eq. (32) is:

$$\Pi = \frac{1}{2}\{a\}^T [K]\{a\} + \frac{1}{2}\{a\}^T [G]\{a\} - \{a\}^T [q]$$

where $\{a\}$ represents the coefficients of the basis functions; $[K]$ is the stiffness matrix; $[G]$ is called the geometric stiffness matrix, and $\{q\}$ is the load vector. In typical structural stability problems, $T_i=0$, σ_{ij}^0 is predominantly compressive, and the objective is to find the lowest scalar multiplier of σ_{ij}^0, denoted by λ, and the corresponding nontrivial displacement vector function u_i, such that

$$\Pi(u_i) = \frac{1}{2}\int_\Omega C_{ijkl}\varepsilon_{ij}\varepsilon_{kl}dV + \frac{\lambda}{2}\int_\Omega \sigma_{ij}^0 u_{\alpha,i} u_{\alpha,j} dV \tag{33}$$

is minimum. The stress field σ_{ij}^0 is called the *pre-buckling* stress state, and the critical load, also called the bifurcation buckling load, is $\lambda_{min} T_i^0$.

The discretized form of the eigenvalue problem represented by the minimization of Eq. (33) is:

$$([K] + \lambda[G])\{a\} = 0 \tag{34}$$

where the stiffness matrix is computed in the usual way (see Eq. (15)) and the geometric matrix is determined from the second integral in Eq. (32) as follows:

$$\{a\}^T[G]\{a\} = \int_\Omega ((\{D\}u_x)^T[\sigma_0]\{D\}u_x + (\{D\}u_y)^T[\sigma_0]\{D\}u_y + (\{D\}u_z)^T[\sigma_0]\{D\}u_z)dV \quad \text{(35)}$$

where u_x, u_y, u_z are the Cartesian components of the displacements which are related to the curvilinear components through the rotation matrix $[R]$, $\{D\}$ is a differential operator vector and $[\sigma_0]$ is the stress tensor written in matrix form as indicated below.

$$\{D\} = \left\{ \begin{array}{c} \dfrac{\partial}{\partial x} \\ \dfrac{\partial}{\partial y} \\ \dfrac{\partial}{\partial z} \end{array} \right\}, \qquad [\sigma_0] = \begin{bmatrix} \sigma_x & \tau_{xy} & \tau_{xz} \\ \tau_{yx} & \sigma_y & \tau_{yz} \\ \tau_{zx} & \tau_{zy} & \sigma_z \end{bmatrix}$$

The implementation of this algorithm in the prototype software requires two steps for the computation of the buckling load factor:

- A linear elastostatic problem is solved first for the specified loadings (T_i^0) and constraints. The linear solution is used to compute the initial stress tensor σ_{ij}^0. The stress tensor σ_{ij}^0 at each integration point is used to compute the geometric matrix.

- After the geometric matrix is available, the eigenvalue problem represented by Eq. (34) is solved to find the minimum buckling load factor. The critical load is then: $T_{cr} = \lambda_{min} T_i^0$.

Several model problems of homogeneous and laminated shells have been solved using the algorithm described above. The results indicate that the implementation provides very accurate results when compared with data published in the literature and with the results of fully three-dimensional analysis. An unique feature of the formulation is that it is not tied to a particular type of dimensional reduction but rather it can be used in conjunction with the hierarchic family of models and even for fully tree-dimensional models.

2.3.3 Pre-stress modal analysis

The formulation for elastic vibration is analogous to Eq. (32) for eigenvalue buckling. Specifically, we seek to find ω and $u_i \in \overset{\circ}{E}(\Omega)$, $u_i \neq 0$ such that

$$\Pi^*(u_i) = \frac{1}{2}\int_\Omega C_{ijkl}\varepsilon_{ij}\varepsilon_{kl}dV + \frac{1}{2}\int_\Omega \sigma_{ij}^0 u_{\alpha,i}u_{\alpha,j}dV - \omega^2\int_\Omega \rho u_i u_i dV \quad \text{(36)}$$

is minimum. The symbols ω and ρ in Eq. (36) represent the natural frequency and the mass density, respectively. The importance of the stress field σ_{ij}^0 is clearly visible from Eq. (36): If σ_{ij}^0 is predomi-

nantly tensile then the stiffness is increased, whereas if $\sigma_{ij}{}^0$ is predominantly compressive then the stiffness is decreased. If $\sigma_{ij}{}^0$ is a buckling stress then the lowest natural frequency is zero.

The discretized form of the potential energy in Eq. (36) is:

$$\Pi^* = \frac{1}{2}\{a\}^T([K]+[G])\{a\} - \omega^2\{a\}^T[M]\{a\}$$

(37)

where, as before, $\{a\}$ represents the coefficients of the basis functions; $[K]$ is the stiffness matrix; $[G]$ is the geometric stiffness matrix, and $[M]$ is the mass matrix. The discretized form of the eigenvalue problem represented by the minimization of Eq. (37) is:

$$([K]+[G]-\lambda[M])\{a\} = 0$$

(38)

where $\lambda=\omega^2$, the stiffness matrix $[K]$ is computed from Eq. (15), the geometric matrix $[G]$ is determined from Eq. (35) and the mass matrix $[M]$ is computed from:

$$\{a\}^T[M]\{a\} = \int_\Omega \rho(u_r^2 + u_s^2 + u_w^2)dV$$

(39)

The implementation of the pre-stress modal analysis in the prototype software requires two steps:

- A linear elastostatic problem is solved first for the specified loadings (T_i^0) and constraints. The linear solution is used to compute the initial stress tensor $\sigma_{ij}{}^0$. The stress tensor $\sigma_{ij}{}^0$ at each integration point is used to compute the geometric matrix.

- The stiffness matrix is modified by the geometric matrix and the mass matrix is also computed to solve the eigenvalue problem of Eq. (38).

Examples problems are presented in the next section.

2.4 Example problems

2.4.1 Problem 1: Linear elastostatic analysis of a cylindrical shell

A cylindrical shell clamped at one end and loaded by a uniform distributed normal traction was analyzed using the 5-field shell model implemented in the prototype software and the results were compared with a 3D-solid finite element solution of the same configuration.

Figure 3 shows the shell model consisting of one quadrilateral shell element and the contour plot of the Uy displacement component. The shell has a radius $R=2.0$, a length $a=2.0$, a width $b=0.5$ and a thickness $h=0.10$. The normal load has a magnitude of $q=100$ and the material is homogenous and isotropic with $E=10\times10^6$ and $\nu=0.0$. The corresponding 3D-solid model, consisting of one hexahedral solid element, and the contour plot of the Uy displacement component are shown in Figure 4.
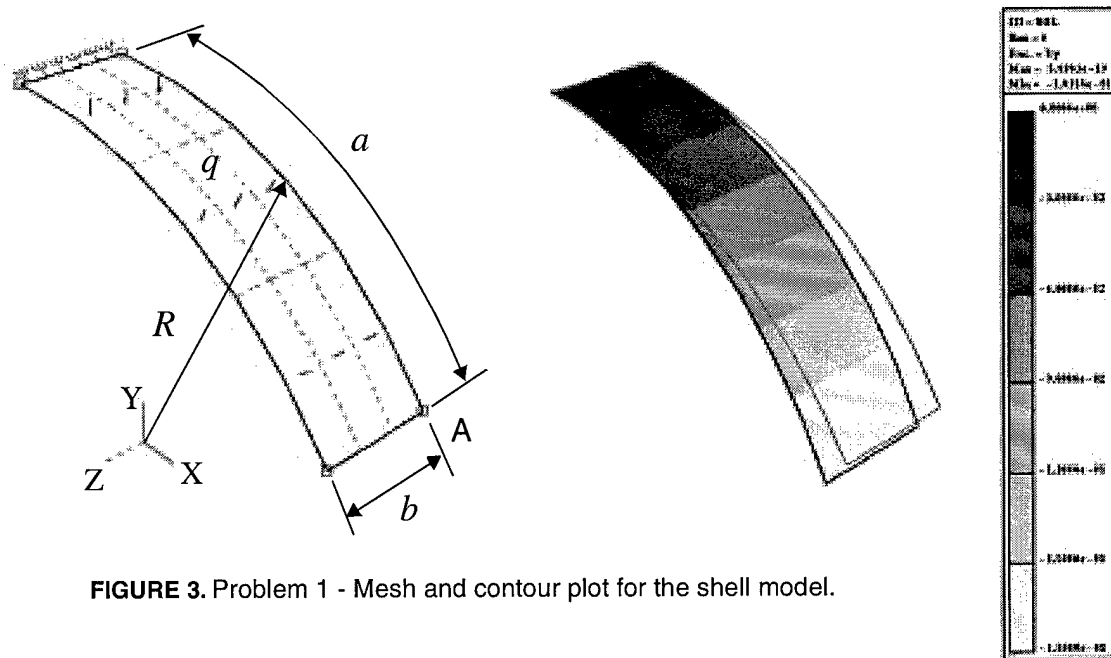
FIGURE 3. Problem 1 - Mesh and contour plot for the shell model.
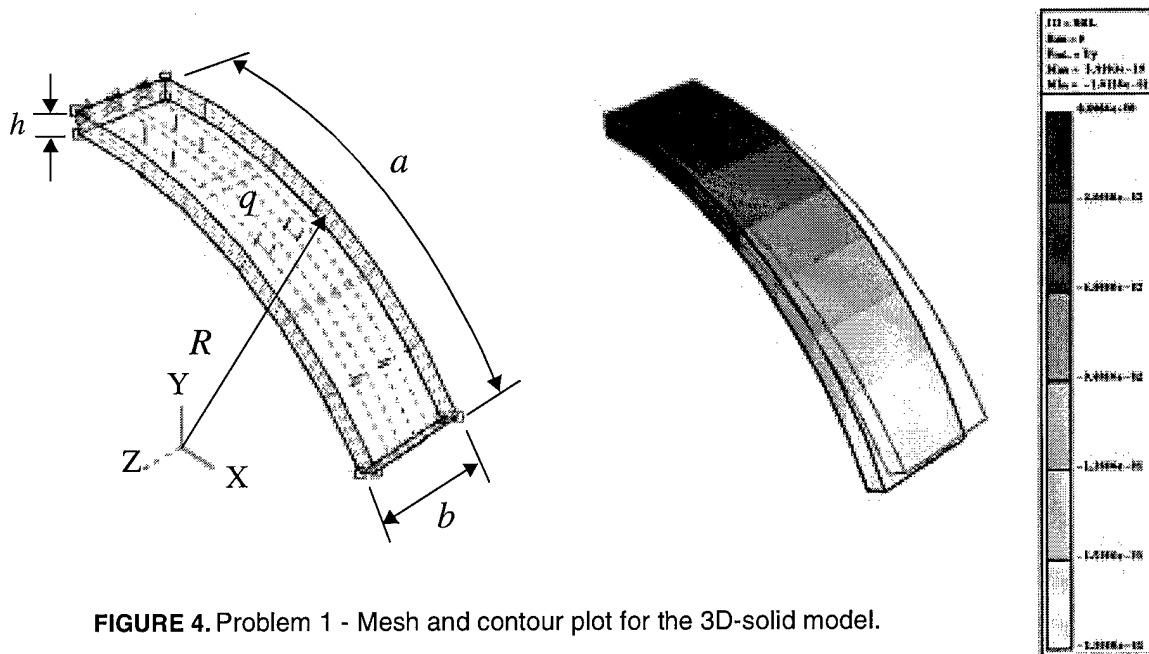
FIGURE 4. Problem 1 - Mesh and contour plot for the 3D-solid model.

The finite element solution was obtained for a fixed finite element mesh and for increasing polynomial order ranging from p=1 to 6 for both models. The estimated error in energy norm for each case is

shown in Figure 5 in tabular form and in a log-log scale plot, where the horizontal axis is the log of
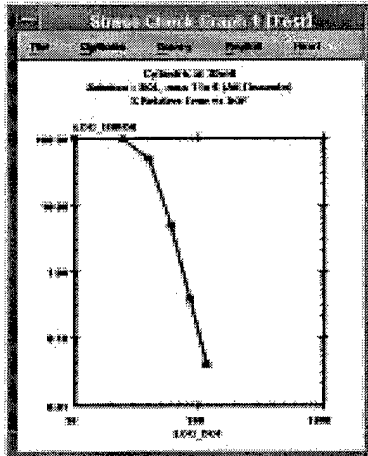
(a) Shell model

```
Error Estimate (All Elements), ID= SOL, run #1 to #6
                                            Rate of        Estimated
Run #        DOF        Total Potential Energy  Convergence    % Error
```

Run #	DOF	Total Potential Energy	Rate of Convergence	Estimated % Error
1	10	-2.389949952653914e-02	0.00	99.72
2	25	-4.120727750166704e-01	0.05	95.05
3	40	-3.285389747569158e+00	1.45	48.02
4	60	-4.259780965826461e+00	5.63	4.90
5	85	-4.269957708088871e+00	7.40	0.37
6	115	-4.270015928027199e+00	7.40	0.04

Estimated Limit	-4.270016597868776e+00

(b) 3D-solid model

```
Error Estimate (All Elements), ID= SOL, run #1 to #6
                                            Rate of        Estimated
Run #        DOF        Total Potential Energy  Convergence    % Error
```

Run #	DOF	Total Potential Energy	Rate of Convergence	Estimated % Error
1	12	-2.115019881502798e-02	0.00	99.75
2	36	-1.379345240360249e-01	0.01	98.37
3	60	-2.589890171918026e+00	0.88	62.76
4	99	-4.212006486270239e+00	3.32	11.93
5	153	-4.270967693800999e+00	4.03	2.07
6	225	-4.272710128732996e+00	4.03	0.44

| Estimated Limit	-4.272791785275626e+00
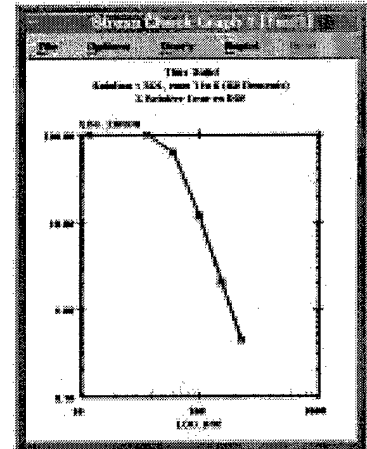
FIGURE 5. Problem 1 - Estimated relative error in energy norm.

the number of degrees of freedom (DOF) and the vertical axis is the log of the percent estimated relative error in energy norm. Note that the DOF for the shell model is smaller than for the 3D-solid model for the same run number (p-level), and the rate of convergence increases substantially for p-level greater than or equal to 4. The shell model is converging to the same potential energy as the reference three-dimensional solution given by the 3D-solid model.

The displacement of point A (Figure 3) at the free end of the shell mid-surface is shown in Figure 6 for the shell model (Figure 6a) and for the reference 3D-solid solution (Figure 6b) as a function of the run number. The results for both models are almost identical. The difference between the shell model and the 3D-solid model is only 0.04% for the Ux displacement component and 0.05% for Uy component. Figure 7 shows the convergence characteristics of the displacement component Uy as a function of the number of degrees of freedom (DOF) for the shell model.

```
Point Function, ID= SOL, run #1 to 6                    (a) Shell model
---------------------------------------------------------------------------
n=     4, x= 1.68294e+00, y= 1.08060e+00, z= 0.00000e+00, Ux=-5.46170e-04 , Uy=-9.18733e-04
n=     4, x= 1.68294e+00, y= 1.08060e+00, z= 0.00000e+00, Ux=-1.49293e-02 , Uy=-1.93801e-02
n=     4, x= 1.68294e+00, y= 1.08060e+00, z= 0.00000e+00, Ux=-1.06430e-01 , Uy=-1.46425e-01
n=     4, x= 1.68294e+00, y= 1.08060e+00, z= 0.00000e+00, Ux=-1.24992e-01 , Uy=-1.81503e-01
n=     4, x= 1.68294e+00, y= 1.08060e+00, z= 0.00000e+00, Ux=-1.24740e-01 , Uy=-1.81582e-01
n=     4, x= 1.68294e+00, y= 1.08060e+00, z= 0.00000e+00, Ux=-1.24741e-01 , Uy=-1.81584e-01


Point Function, ID= SOL, run #1 to 6                    (b) 3D-Solid model
---------------------------------------------------------------------------
n=     2, x= 1.68294e+00, y= 1.08060e+00, z= 8.75886e-15, Ux=-4.90053e-04 , Uy=-7.21372e-04
n=     2, x= 1.68294e+00, y= 1.08060e+00, z= 8.75886e-15, Ux=-4.28834e-03 , Uy=-5.92515e-03
n=     2, x= 1.68294e+00, y= 1.08060e+00, z= 8.75886e-15, Ux=-9.11811e-02 , Uy=-1.20099e-01
n=     2, x= 1.68294e+00, y= 1.08060e+00, z= 8.75886e-15, Ux=-1.25888e-01 , Uy=-1.80942e-01
n=     2, x= 1.68294e+00, y= 1.08060e+00, z= 8.75886e-15, Ux=-1.24780e-01 , Uy=-1.81632e-01
n=     2, x= 1.68294e+00, y= 1.08060e+00, z= 8.75886e-15, Ux=-1.24793e-01 , Uy=-1.81682e-01
```

FIGURE 6. Problem 1 - End displacement components Ux and Uy.
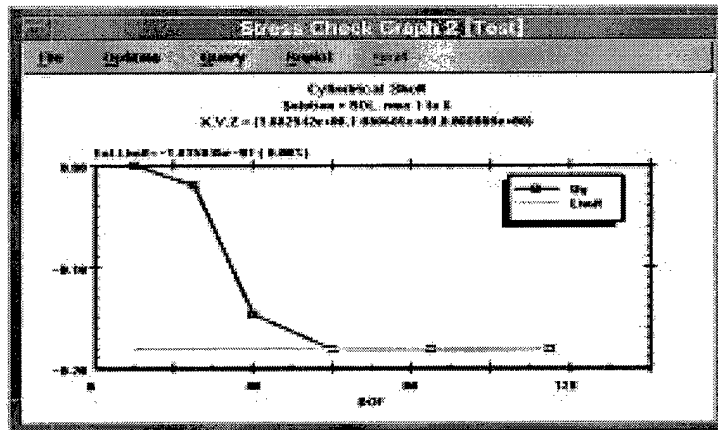
FIGURE 7. Problem 1 - Convergence plot of Uy for the shell model.

This example demonstrates some of the key features of the implementation of the first shell model into the prototype software: Quality of approximation of the three-dimensional problem; global error assessment capability; and local error assessment thorough convergence checks.

2.4.2 Problem 2: Geometric nonlinear analysis of a slab

Consider the case of a rectangular slab clamped along one edge and loaded by a uniformly distributed normal traction, as shown in Figure 8a. The load remains normal to the plate surface during the defor-

(a) Plate configuration

Iteration

(b) Linear solution

(c) Nonlinear solution
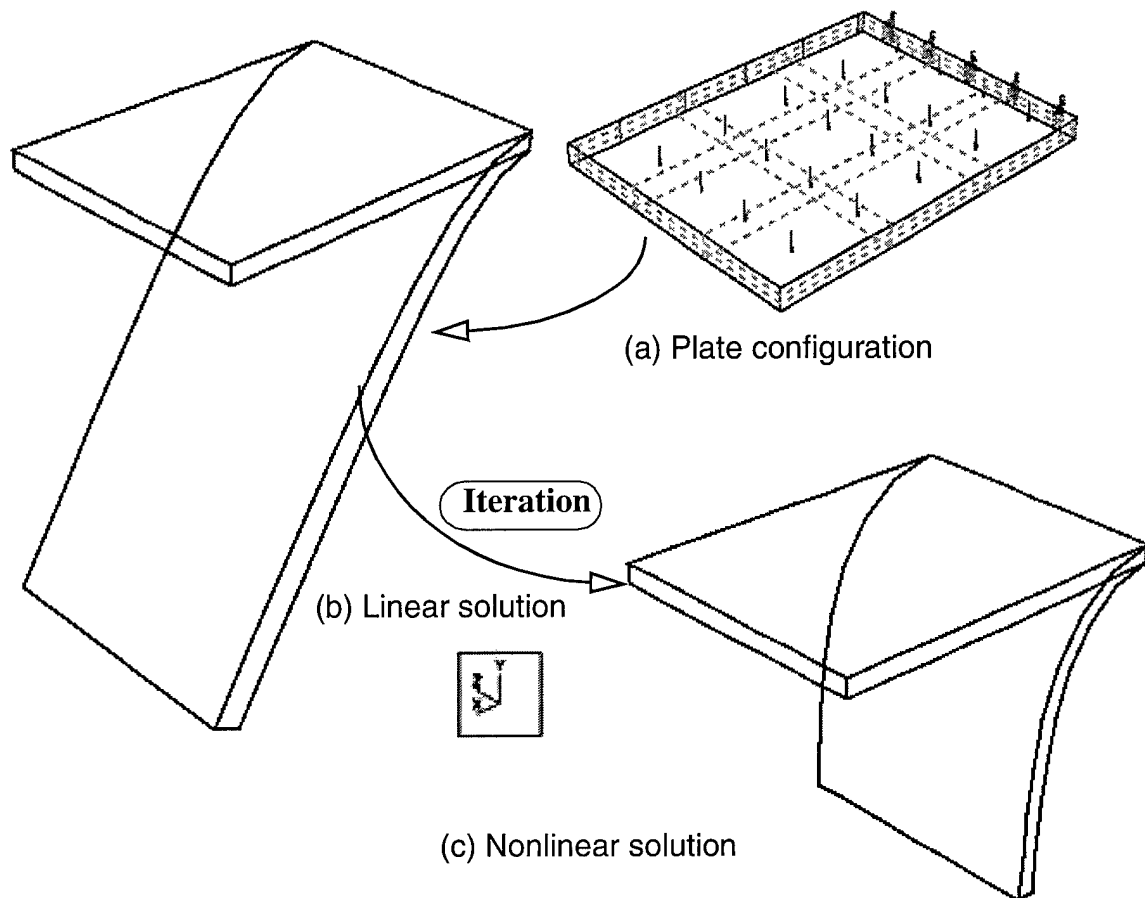
FIGURE 8. Problem 2 - Geometric nonlinear analysis.

mation ('follower' load). Figure 8b shows the deformed configuration of the plate (full scale) for the linear solution. It is clear form the results that the deformation obtained from the linear solution is outside of the range of validity of the linear theory of elasticity. Figure 8c shows the deformation (full scale) obtained with the geometrically nonlinear formulation implemented in the prototype software.

2.4.3 Problem 3: Buckling and modal analysis of a roof structure

Consider the cylindrical roof structure shown in Figure 9. The shell is of sandwich construction, with the outer layers of high modulus graphite/epoxy composite material and an isotropic material core. A vertical dead load is applied to the roof, and the objective of the analysis is to determine the maximum vertical deflection, the largest normal stress, the first natural frequency of vibration and the buckling load factor. Also of interest is to determine the change in natural frequency as a function of the load magnitude.
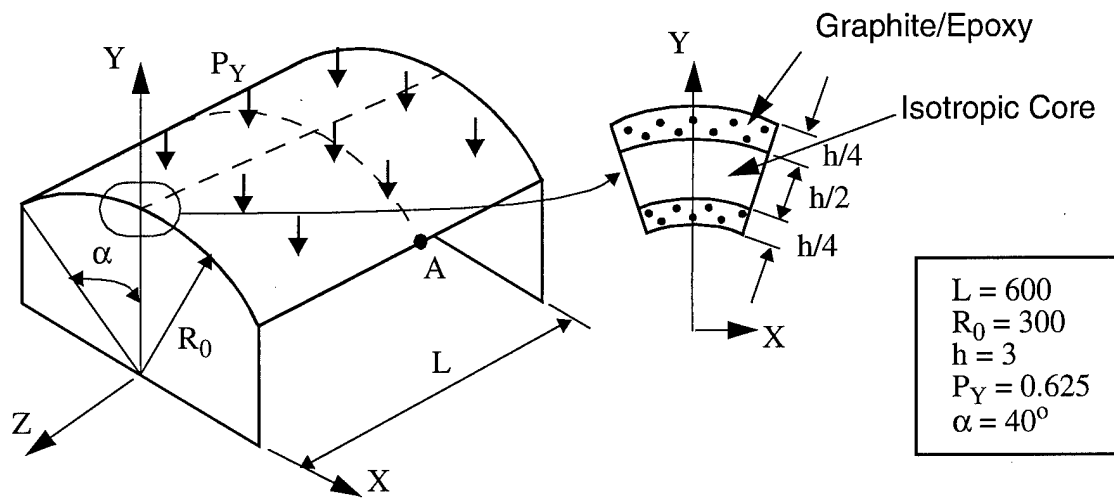
FIGURE 9. Problem 3 - Cylindrical roof structure. Notation.

The following material properties were used for the external layers and core:

Graphite/Epoxy: E_L=25x10^6; E_T =1x10^6; G_{LT} =5x10^5; G_{TT} =2x10^5; v_{LT}= v_{TT} =0.3, ρ=1x10^{-4}

Isotropic: E=3x10^6; v=0.0; ρ=1x10^{-4}

where L indicates the direction parallel to the fibers and T is the transverse direction. In this problem, the L-direction is aligned with the global Z-axis. Because of symmetry, only one fourth of the roof was included in the analysis. The problem was solved using the first hierarchic shell model and also using a 3D-solid model in order to have a reference solution. Figure 10 shows the 2-element mesh for the shell model and the 6-element mesh for the 3D-solid model. In the solid model, each layer was discretized using hexahedral elements.

Symmetry boundary conditions (u_n=0, where u_n is the displacement normal to the edge) were specified along two orthogonal directions, and antisymmetry boundary conditions (u_w=u_t=0, where u_t is the displacement tangent to the edge) were used to represent the effects of the end support. The other edge is free. Note that a thin element was defined along the free edge of the shell and 3D-solid models to properly account for boundary layer effects. The results, obtained from shell model 1 and from the 3D-solid model, are summarized in Table 1. They include the maximum vertical displacement, u_y^A(x_A,y_A,z_A), where (x_A, y_A, z_A) are the coordinates of the shell mid-surface at point A (see Figure 9); the normal stresses at point A on the lower surface of the roof, σ_z^A; the first natural frequency without pre-stress, f_1, and the buckling load factor, *BLF*. The last row in the table are the value of the critical
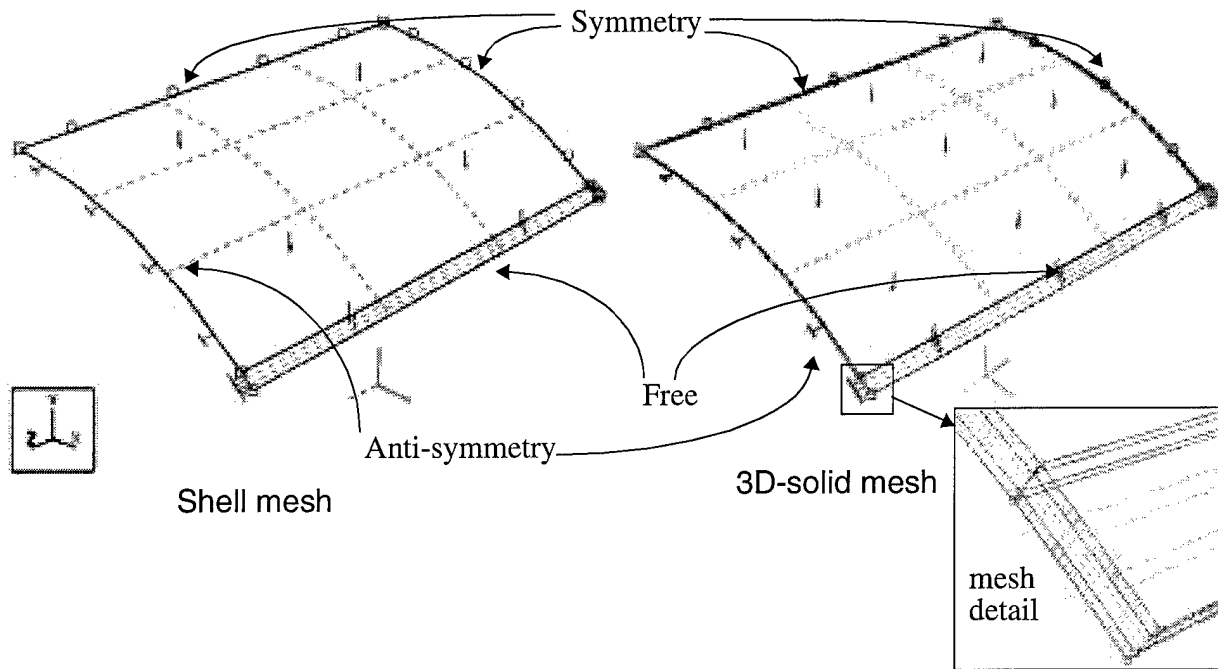
FIGURE 10. Problem 3 - Finite element meshes.

load on the roof, which were computed as the product of the applied load (P_Y=0.625) and the buckling load factor (*BLF*).

TABLE 1. Results for problem 3

Function	Shell model 1	3D-solid model	Difference (%)
$u_y{}^A$	-2.73	-2.82	-3.2
$\sigma_z{}^A$	10614	10843	-2.1
f_1 [Hz]	4.71	4.64	1.5
BLF	11.29	10.39	8.7
$(P_Y)_{CR}$	7.06	6.49	8.7

The results of shell model 1 are very close to those obtained using the 3D-solid model specially for the linear and modal analysis results. Figure 11 shows the buckling mode shape for both models. The effect of the pre-stress induced by the applied load (P_Y) on the first natural frequency of the roof

Shell model   3D-solid model
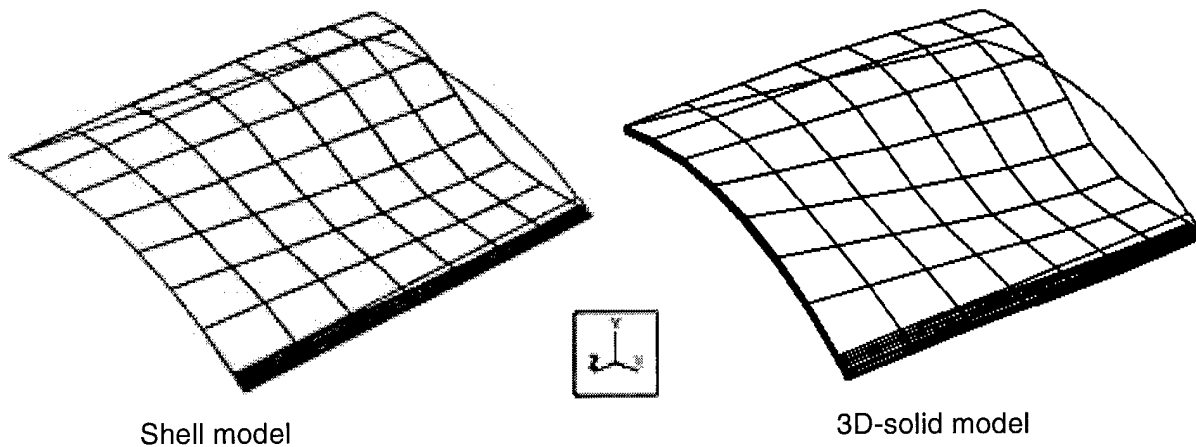
FIGURE 11. Problem 3 - Buckling mode shape

structure was obtained for the shell model, and the results are included in Table 2. The pre-stress

TABLE 2. Effect of pre-stresses on the first natural frequency

P_Y	0.0	1.0	2.0	3.0	4.0	5.0	6.0	6.5	7.0	7.06
f_1 [Hz]	4.71	5.39	5.82	6.01	5.89	5.31	4.07	3.02	0.95	0.00

increases the natural frequency until the load is about half the critical load, and then decreases rapidly as the critical buckling load is approached.

3.0 Higher order models

Hierarchic sequence of models satisfy the equilibrium equations of three-dimensional elasticity to the desired degree of accuracy. In the limit it converges to the fully three-dimensional solution. Depending on the goals of computation, the analyst can select the model that best fits the goals. Choosing progressively higher models, the computational effort increases, but of course the accuracy in the results is improved also. If only structural response is required, a low-order model is generally sufficient, specially for thin shells. Hierarchic sequences of models make adaptive selection of the model which is best suited for the purposes of a particular analysis possible.

3.1 Concept and terminology

The first rigorous proof of the relation between the three-dimensional solution and a plate model was given by Morgenstern, Ref. [11], in 1959. The construction of hierarchic models for homogeneous isotropic plates and shells was discussed by Szabo and Sahrmann in 1988, Ref. [12]. The optimality conditions for the construction of the hierarchic models for homogeneous plates was first discussed

by Schwab in 1989, Ref. [13]. The extensions of these concepts for laminated composites was first addressed in Ref. [14] for plates in cylindrical bending, in Ref. [16] for general plates with mid-plane symmetry, and in Ref. [17] for laminated shells.

Hierarchic modeling terminology has been used by other authors (see for example Ref. [19]) but in a context which is different from ours. As we understand it, a hierarchic sequence of models is properly formulated if satisfies the condition that the corresponding exact solutions $u_{EX}^{(HM|i)}$, converge to the exact solution of the fully 3D-problem $u_{EX}^{(3D)}$, for a fixed laminate thickness,

$$\lim_{i \to \infty} \left\| u_{EX}^{(3D)} - u_{EX}^{(HM|i)} \right\|_{E(\Omega)} = 0$$

where $E(\Omega)$ is the energy norm. In addition, they should posses two highly desirable features:

1. The exact solution of each model converges to the same limit as the exact solution of the corresponding 3D-problem with respect to the laminate thickness (h) approaching zero:

$$\lim_{h \to 0} \frac{\left\| u_{EX}^{(3D)} - u_{EX}^{(HM|i)} \right\|_{E(\Omega)}}{\left\| u_{EX}^{(3D)} \right\|_{E(\Omega)}} = 0, \qquad i = 1, 2, \dots$$

This requirement is important because, typically, $u_{EX}^{(3D)}$ in the interior regions of the domain behaves as if h were close to zero, assuming that the loading is smooth.

2. Optimality of convergence: When the exact solution $u_{EX}^{(3D)}$ is sufficiently smooth:

$$\frac{\left\| u_{EX}^{(3D)} - u_{EX}^{(HM|i)} \right\|_{E(\Omega)}}{\left\| u_{EX}^{(3D)} \right\|_{E(\Omega)}} \approx Ch^{\gamma_i}$$

where C is a constant, independent of i; γ, the rate of convergence, is a constant which depends on i, and $\gamma_{i+1} > \gamma_i$.

The hierarchic sequence utilized for the Phase I project for laminated plates and the one developed during Phase II for laminated shells, satisfy these requirements explicitly.

3.2 Transverse shape functions for hierarchic shell models

Two high-order (hierarchic) shell models for homogeneous and laminated composites were developed and implemented within the framework of the finite element software product Stress Check. The transverse shape functions developed for laminated plates (see Ref. [17]) were reevaluated and modified to be used for laminated shells. Six new shape functions and their derivatives are available.

As described in Section 2.0, the first hierarchic shell model is a five-field semi-discretization which approximates the curvilinear components of the displacement vector as indicated in Eq. (1). The expansion of the three displacement components to include two additional models can be written in general form as:

$$u_r(r, s, w) = u|_0^r(r, s)\Phi_1(w) + u|_1^r(r, s)\Phi_3(w) + u|_2^r(r,s)\Phi_6(w) + u|_3^r(r,s)\Phi_9(w)$$

$$u_s(r, s, w) = u|_0^s(r, s)\Phi_2(w) + u|_1^s(r, s)\Phi_4(w) + u|_2^s(r,s)\Phi_7(w) + u|_3^s(r,s)\Phi_{10}(w) \qquad (40)$$

$$u_w(r, s, w) = u|_0^w(r, s)\Phi_5(w) + u|_1^w(r, s)\Phi_8(w) + u|_2^w(r,s)\Phi_{11}(w)$$

where the $\Phi_i(w)$ are the transverse shape functions (director functions) which depend on the variable normal to the shell middle surface and on the type of shell (homogenous or laminated). Note that there is a change in notation with respect to that shown in Eq. (1). The unknown functions of (r, s) are identified with a subscript that indicated a sequential order, and by a superscript which refers to the corresponding displacement component, while the known functions of w are numbered to reflect the sequence of model construction.

The transverse shape functions are obtained according the following procedure:

Let $u_r(r, s, w)$, $u_s(r, s, w)$, $u_w(r, s, w)$ denote the displacement field for the shell composed of an arbitrary number of orthotropic layers bonded together subjected to normal surface loading $T_i(r, s)$ and satisfying the equilibrium equations of 3D-elasticity. Let the stresses be related to the strains by the generalized Hooke's law, and the strains related to the displacements by the small strain theory. The problem is to find the displacement field that minimizes the potential energy functional $\Pi(u)$ over the subspace $E^n(\Omega)$, defined as:

$$E^n(\Omega) = \left\{ \vec{u} \,\middle|\, u_r(r,s,w) = \sum_{j=0}^{n_1} u|_j^r(r,s)\varphi_j(w), \quad u_s(r,s,w) = \sum_{j=0}^{n_2} u|_j^s(r,s)\psi_j(w), \right.$$
$$\left. u_w(r,s,w) = \sum_{j=0}^{n_3} u|_j^w(r,s)\rho_j(w) \right\}$$

The functions $\varphi_j(w)$, $\psi_j(w)$, $\rho_j(w)$ are derived on the basis of the degree to which the equilibrium equations of 3D-elasticity are satisfied. The procedure to obtain these functions is similar to the one outlined in Refs. [14] - [18] for laminated plates in bending. The main step in the derivation for laminated shells are as follows:

- Perform a partial Fourier transform, with parameters β over the domain Ω of the three-dimensional problem described above. This transformation eliminates two field variables (r, s) in the displacement components, so that derivatives with respect to r and s become multiplications by $i\beta$ in the Fourier transformed variables.

$$\varphi(\beta,w) = \int_A u_r(r,s,w)e^{-i\beta(r+s)}dA$$

$$\psi(\beta,w) = \int_A u_s(r,s,w)e^{-i\beta(r+s)}dA$$

$$\rho(\beta,w) = \int_A u_w(r,s,w)e^{-i\beta(r+s)}dA$$

- Write down the strain-displacement relations in the transformed variables, substitute them into the stress-strain relations and express the equilibrium equations in their Fourier form. A system of ordinary differential equations is obtained in the variable w.

- Expand the functions $\varphi(\beta,w)$, $\psi(\beta,w)$, $\rho(\beta,w)$ in powers of β around $\beta=0$.

$$\varphi(\beta,w) = \varphi_0(w) + \beta\varphi_1(w) + \beta^2\varphi_2(w) + \beta^3\varphi_3(w) + \dots$$

$$\psi(\beta,w) = \psi_0(w) + \beta\psi_1(w) + \beta^2\psi_2(w) + \beta^3\psi_3(w) + \dots$$

$$\rho(\beta,w) = \rho_0(w) + \beta\varphi_1(w) + \beta^2\rho_2(w) + \beta^3\rho_3(w) + \dots$$

- Replace the expanded functions into the Fourier form of the equilibrium equations, which must be satisfied for any power of β. The transverse shape functions are obtained by solving these equations. For example, the equilibrium equations corresponding to β^0 are:

$$(Q_{45}\psi_0' + Q_{55}\varphi_0')' = 0$$

$$(Q_{44}\psi_0' + Q_{45}\varphi_0')' = 0$$

$$(Q_{33}\rho_0')' = 0$$

- After the functions are obtained by integration of the equilibrium equations, they are normalized in such a way that all functions are zero at $w=0$ and also a thickness factor is included. For consistency of notation, the normalized transverse functions are defined as $\Phi_i(w)$, $i=1, 2, 3, \dots$

The transverse shape functions for laminated shells depend on the stacking sequence layup and on Q_{ij}, which are the coefficients of the 3D-lamina material matrix in the shell principal directions.

For *shell model* 1, the transverse shape functions are the same for laminated or homogeneous material. Referring to Eq. (1), they are given by:

$$\Phi_1(w) = \Phi_2(w) = \Phi_5(w) = 1, \quad \Phi_3(w) = \Phi_4(w) = w(h/2)$$

where h is the shell thickness, and $-1 \le w \le 1$. For the higher order models, the transverse shape functions are defined as follows:

For homogeneous shells

$$\Phi_6(w) = \Phi_7(w) = w^2(h/2)^2, \quad \Phi_8(w) = w(h/2)$$

$$\Phi_9(w) = \Phi_{10}(w) = w^3(h/2)^3, \quad \Phi_{11}(w) = w^2(h/2)^2$$

For laminated shells

$$\Phi_6(w) = \frac{h}{2}\{\varphi_2(w) - \varphi_2(0)\} \qquad \Phi_9(w) = \left(\frac{h}{2}\right)^2 \varphi_3(w)$$

$$\Phi_7(w) = \frac{h}{2}\{\psi_2(w) - \psi_2(0)\} \qquad \Phi_{10}(w) = \left(\frac{h}{2}\right)^2 \psi_3(w)$$

$$\Phi_8(w) = \frac{h}{2}\{\rho_1(w) - \rho_1(0)\} \qquad \Phi_{11}(w) = \left(\frac{h}{2}\right)^2 \rho_2(w)$$

where

$$\varphi_2(w) = \int_{-1}^{w} \frac{Q_{44} - Q_{45}}{Q_{44}Q_{55} - Q_{45}^2} dw \qquad \psi_2(w) = \int_{-1}^{w} \frac{Q_{55} - Q_{45}}{Q_{44}Q_{55} - Q_{45}^2} dw$$

$$\rho_1(w) = \int_{-1}^{w} \frac{1}{Q_{33}} dw$$

It is clear from the above expressions that if Q_{ij} are constant within each lamina but different from lamina to lamina, the transverse variation of $\varphi_2(w)$, $\psi_2(w)$, $\rho_1(w)$ is piecewise linear, and the slope ate each interface depends on the material properties of each layer.

The other three functions are:

$$\varphi_3(w) = \int_{-1}^{w} \left(\rho_1(w) + \frac{Q_{44}\gamma_a(w)}{Q_{44}Q_{55} - Q_{45}^2} - \frac{Q_{45}\gamma_b(w)}{Q_{44}Q_{55} - Q_{45}^2} \right) dw - \int_{-1}^{0} \left(\rho_1(w) + \frac{Q_{44}\gamma_a(w)}{Q_{44}Q_{55} - Q_{45}^2} - \frac{Q_{45}\gamma_b(w)}{Q_{44}Q_{55} - Q_{45}^2} \right) dw$$

$$\psi_3(w) = \int_{-1}^{w} \left(\rho_1(w) + \frac{Q_{55}\gamma_b(w)}{Q_{44}Q_{55} - Q_{45}^2} - \frac{Q_{45}\gamma_a(w)}{Q_{44}Q_{55} - Q_{45}^2} \right) dw - \int_{-1}^{0} \left(\rho_1(w) + \frac{Q_{55}\gamma_b(w)}{Q_{44}Q_{55} - Q_{45}^2} - \frac{Q_{45}\gamma_a(w)}{Q_{44}Q_{55} - Q_{45}^2} \right) dw$$

$$\rho_2(w) = \int_{-1}^{w} \left(\frac{2w}{Q_{33}} + \frac{(Q_{13} + Q_{36})\varphi_2(w)}{Q_{33}} - \frac{(Q_{23} + Q_{36})\psi_2(w)}{Q_{33}} \right) dw - \int_{-1}^{0} \left(\frac{2w}{Q_{33}} + \frac{(Q_{13} + Q_{36})\varphi_2(w)}{Q_{33}} - \frac{(Q_{23} + Q_{36})\psi_2(w)}{Q_{33}} \right) dw$$

$$\gamma_a(w) = \int_{-1}^{w} \frac{Q_{13} + Q_{36}}{Q_{33}} dw - \int_{-1}^{0} \frac{Q_{13} + Q_{36}}{Q_{33}} dw, \qquad \gamma_b(w) = \int_{-1}^{w} \frac{Q_{23} + Q_{36}}{Q_{33}} dw - \int_{-1}^{0} \frac{Q_{23} + Q_{36}}{Q_{33}} dw$$

In this case, the transverse variation is piecewise quadratic.

Several procedures have been evaluated for selecting the optimal distribution of fields for a given problem. Starting with the minimal number of fields (5-field model), the question is how to construct the next model? Our research indicated that from an implementation and performance point of view, the next model should be constructed by adding one more field to each displacement component (u_r, u_s, u_w), and that the transverse function for the r and s components should have the same power of w. In other words, model 2 should be an 8-field semi-discretization with the selection of the three new fields from the available set in Eq. (40).

3.3 Automatic selection of models

The optimal selection of a particular model form the hierarchic family of models is problem-dependent. Starting with a 5-field model, the next model is constructed by adding one more field to each displacement component, in such a way that model 2 has eight fields and model 3 has eleven. Several methods were evaluated to select the best shape functions from the available set to construct the next higher order model: The alternating projection method; the residuals method and the potential energy methods. These methods are described in detail in the following.

3.3.1 The alternating projection method

The alternating projection consists of three parts: First, the solution corresponding to the lowest member of the hierarchy is computed (the 5-field semi-discretization). Second, the part of the solution which depends on the transverse variable (w in Eq. (1)) is expanded in terms of the known transverse shape functions over each element. A one-dimensional problem is solved to find which of these terms in the expansion may contribute to a significant change in the potential energy of the solution. Third, the model order within each element of the mesh is adjusted based on the results of Part 2, and the problem is solved again for the new model distribution. These three steps are now described in detail:

Step 1: Start with the 5-field model for all the elements in the mesh. Obtain the finite element solution corresponding to this model as described in Section 2.0. Note that in this step we solve a two-dimensional problem, because the transverse variation of displacements is know a-priori. The results of this step are the coefficients a_i in Eq. (14). Therefore, for every element in the mesh we know:

$$u\big|_0^r(r, s), \qquad u\big|_0^s(r, s), \qquad u\big|_1^r(r, s), \qquad u\big|_1^s(r, s), \qquad u\big|_0^w(r, s)$$

Step 2: Expand the displacement field given in Eq. (1) in terms of the transverse shape functions shown in Eq. (40) over each element of the mesh:

$$u_r(r, s, w) = u\big|_0^r(r, s) + u\big|_1^r(r, s)(\Phi_3(w) + \alpha_1^{(k)}\Phi_6(w) + \alpha_2^{(k)}\Phi_9(w) + \ldots)$$

$$u_s(r, s, w) = u\big|_0^s(r, s) + u\big|_1^s(r, s)(\Phi_4(w) + \beta_1^{(k)}\Phi_7(w) + \beta_2^{(k)}\Phi_{10}(w) + \ldots) \tag{41}$$

$$u_w(r, s, w) = u\big|_0^w(r, s)(\Phi_5(w) + \gamma_1^{(k)}\Phi_8(w) + \gamma_2^{(k)}\Phi_{11}(w) + \ldots)$$

The transverse shape functions $\Phi i(w)$ are those obtained in Section 3.2. Therefore, the only unknowns in Eq. (41) are the coefficients α_i, β_i and γ_i that multiply these functions. The superscript k indicates the kth finite element.

This new displacement field is then used in Eq. (10) to obtain a new system of equations to solve for the unknown coefficients in Eq. (41). Note that the new system corresponds to a one-dimensional problem in the transverse direction since the only unknowns in the expanded displacement field are the coefficient that multiply the transverse functions. The system size is $3 \times N \times M$, where M is the number of elements in the mesh, and N is the total number of unknown coefficients in Eq. (41). The relative magnitudes of the coefficients will indicate which additional terms will contribute most significantly to the potential energy of the solution.

Step 3: Expand the model order over each element or groups of elements according to the relative values of the coefficients α_i, β_i and γ_i that multiply the transverse functions. Once the number of fields are known, the solution of the corresponding 2D problem is obtained for the selected higher-order model.

The name *alternating projection* comes from the fact that the three-dimensional problem is solved by first minimizing the potential energy of a two-dimensional problem (projection from 3D to 2D), then using that solution to set up a one-dimensional problem in the transverse direction (projection from 3D to 1D), whose solution is finally used to reformulate the 2D minimization problem.

3.3.2 The residuals method

The residuals method consists of the following steps:

Step 1: Start with the 5-field model for all the elements in the mesh. Obtain the finite element solution corresponding to this model as described in Section 2.0. This step is the same as in the previous method.

Step 2: Consider a candidate model 2 from the available set in Eq. (40). For example, we may consider the following displacement field:

$$u_r(r, s, w) = u|_0^r(r, s)\Phi_1(w) + u|_1^r(r, s)\Phi_3(w) + u|_2^r(r,s)\Phi_6(w)$$

$$u_s(r, s, w) = u|_0^s(r, s)\Phi_2(w) + u|_1^s(r, s)\Phi_4(w) + u|_2^s(r,s)\Phi_7(w) \tag{42}$$

$$u_w(r, s, w) = u|_0^w(r, s)\Phi_5(w) + u|_2^w(r,s)\Phi_{11}(w)$$

from which is possible to compute the stiffness matrix and load vector using the displacement field of Eq. (42) into Eq. (10). The resulting system of equations can be written as:

$$[K]_{(2a)}\{a\}_{(2a)} = \{q\}_{(2a)} \tag{43}$$

where the subscript $2a$ indicates that Eq. (43) refers to the system of equations for candidate model 2 combination a. Note that the size of the solution vector $\{a\}$ is larger than that of Eq. (14) because the number of fields is now eight instead of five. Compute the residuals which are defined as:

$$\{R\}_{(2a)} = \{q\}_{(2a)} - [K]_{(2a)}\{\tilde{a}\}_1 \tag{44}$$

where $\{\tilde{a}\}_1$ is the solution vector corresponding to model 1 augmented by zeros in those positions where the terms corresponding to model 2 are needed.

Step 3: Repeat the procedure for other candidate model 2, in such a way that the residuals for each one can be computed: $\{R\}_{(2b)}$, $\{R\}_{(2c)}$, $\{R\}_{(2d)}$,... Compute the norm (vector length) of each residual. The best candidate is the one with the smallest residual norm.

Note that the solution of the system of equations in (43) is not needed, only the stiffness matrices and load vectors of the candidate models are required.

3.3.3 The potential energy method

This criterion for model selection is based on the change in the value of the total potential energy of the problem. The combination of additional fields that results in the smallest potential energy provides the best improvement over the solution of model 1.

The procedure for selecting the optimal distribution of fields for a given problem consists of two steps:

Step 1: The basic model (5-field semi-discretization) is increased by adding one more field to each displacement component (u_r, u_s, u_w), in such a way that the transverse function for the r and s components have the same order of director function. In other words, model 2 should be an 8-field semi-discretization.

Step 2: The criterion for selecting which of the available director functions should be added is based on the change in the value of the total potential energy of the problem. Those directors functions which result in the smallest potential energy will provide the best improvement over the solution of the 5-field model. The potential energy accounts for the effects of topology, material properties and boundary conditions, thus characterizing the problem. The potential energy is computed by solving the problem several times for each candidate combination of director functions at a low p-level:

$$\Pi = \frac{1}{2}\{a\}^T [K]\{a\} - \{a\}^T [q]$$

To illustrate the concept of model selection, consider the situation of selecting an 8-field model. There are four possible combinations from the expansion given in Eq. (40) for the additional three fields needed to extend the 5-field model: (a) Φ_6, Φ_7, Φ_8; (b) Φ_6, Φ_7, Φ_{11}; (c) Φ_9, Φ_{10}, Φ_8 and (d) Φ_9, Φ_{10}, Φ_{11}. No other combinations are possible, given the constraint on the order of the director functions indicated before. For example, the hierarchic model 2, combination (d) would be:

$$u_r(r, s, w) = u|_0^r(r, s)\Phi_1(w) + u|_1^r(r, s)\Phi_3(w) + u|_2^r(r,s)\Phi_9(w)$$

$$u_s(r, s, w) = u|_0^s(r, s)\Phi_2(w) + u|_1^s(r, s)\Phi_4(w) + u|_2^s(r,s)\Phi_{10}(w)$$

$$u_w(r, s, w) = u|_0^w(r, s)\Phi_5(w) + u|_2^w(r,s)\Phi_8(w)$$

Of all the methods evaluated, the one based on the minimization of the total potential energy of the problem was selected for implementation into the prototype software because it was the simplest and

most effective of the ones analyzed. The computational effort to determine the optimal set of director functions is minimized when using this method. The automatic procedure implemented in the proto-type software will solve for each combination at p-level=4, and select that one which minimizes the potential energy of the problem. Once the optimal model is identified, a p-extension is performed to ascertain the discretization error.

3.4 Example problems

3.4.1 Problem 4. Thick 4-ply laminate

Consider a 4-ply $[0/90]_s$ laminated plate loaded by a sinusoidal transverse load $q_z(x,y) = -cos(\pi x/a)$ $cos(\pi y/b)$. The four layers of the laminate are of the same material and thickness with the following properties:

$$E_L = 138000 \text{ MPa}; \ E_T = 9300 \text{ MPa}; \ G_{LT} = 4600 \text{ MPa}; \ G_{TT} = 3100 \text{ MPa}; \ \nu_{LT} = 0.3, \ \nu_{TT} = 0.5$$

where L indicates the direction parallel to the fibers and T is the transverse direction. When the L-direction coincides with the x-direction, we refer to it as the $0°$ orientation (Figure 12). All the dimen-sions are in millimeters. The plate is hard-simply supported along all four edges. A hard-simple sup-port is characterized by: $u_z = u_t = 0$, where u_t is the displacement component tangent to the edge, and $u_z = u_w$.
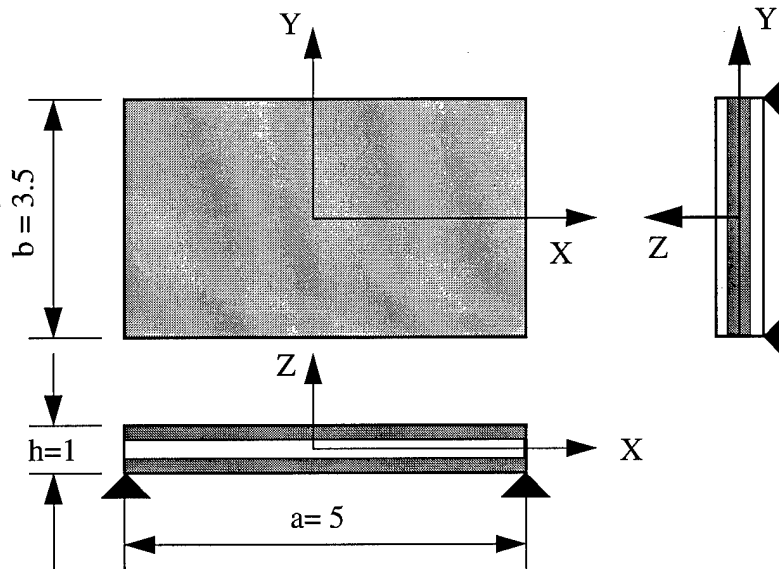

FIGURE 12. Problem 4 - Laminated plate. Notation

The reference solution was obtained from the finite element analysis of a 3D-solid model in which each layer was discretized as a solid element. Because of symmetry, only one quarter of the plate was

used for the shell analysis, and one eighth for the solid analysis. Figure 13 shows the one-element
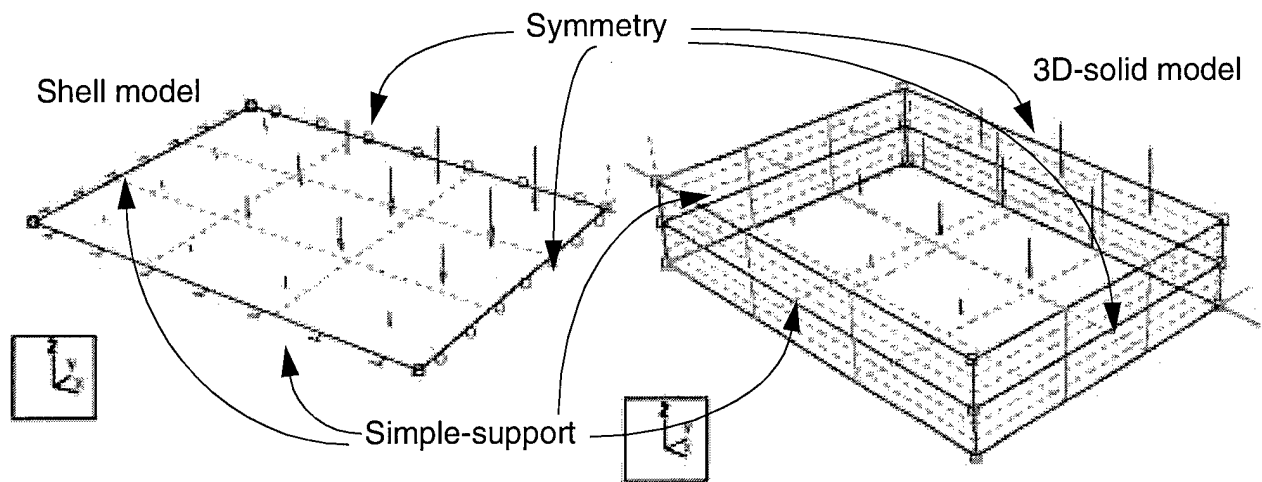
FIGURE 13. Problem 4 - Finite element meshes for the shell and 3D-solid models.

mesh for the shell analysis and the two-element mesh for the 3D-solid analysis. Antisymmetry constraints were specified on the middle surface of the 3D-solid model.

The results for the shell models were obtained for the first and second hierarchic shell models. The optimal combination of transverse shape functions for model 2 to be used in the 8-field semi-discretization of Eq. (40) was determined to be Φ_6, Φ_7, Φ_{11} (as it should be expected for a bending dominated problem).

The results shown in Table 3 include the total potential energy of the solution $\Pi(u)$; the maximum displacement at the center of the plate $u_z(0,0,0)$; the normal stresses $\sigma_x(0,0,-h/2)$ and $\sigma_y(0,0,-h/2)$ and the shear stress $\tau_{xy}(a/2,b/2,-h/2)$ at one of the external surfaces of the plate for both hierarchic shell models (shell 1 and 2) and for the 3D-solid model.

TABLE 3. Results for problem 4

Model	$\Pi(u) \times 10^4$	$u_z(0,0,0)$	$\sigma_x(0,0,-h/2)$	$\sigma_y(0,0,-h/2)$	$\tau_{xy}(a/2,b/2,-h/2)$
Shell 1	-2.8746631	-5.2565×10^{-4}	6.4389	1.4035	-0.7274
Shell 2	-2.9863590	-5.5671×10^{-4}	7.3924	1.9688	-0.8154
3D-Solid	-3.0850379	-5.7263×10^{-4}	7.7388	1.9267	-0.8602

The low aspect ratio of the plate combined with the highly anisotropic nature of the material represent a severe test for any laminated shell model. The length-to-thickness ratio is only 3.5, and therefore not suitable for conventional shell analysis. However, the use of higher order models indicates that the results converge to the fully three-dimensional solution.

The through-thickness stress distribution of the normal stresses at the center of the plate is shown in Figure 14 for shell models 1 and 2. Differences between the two models is visible at the external sur-
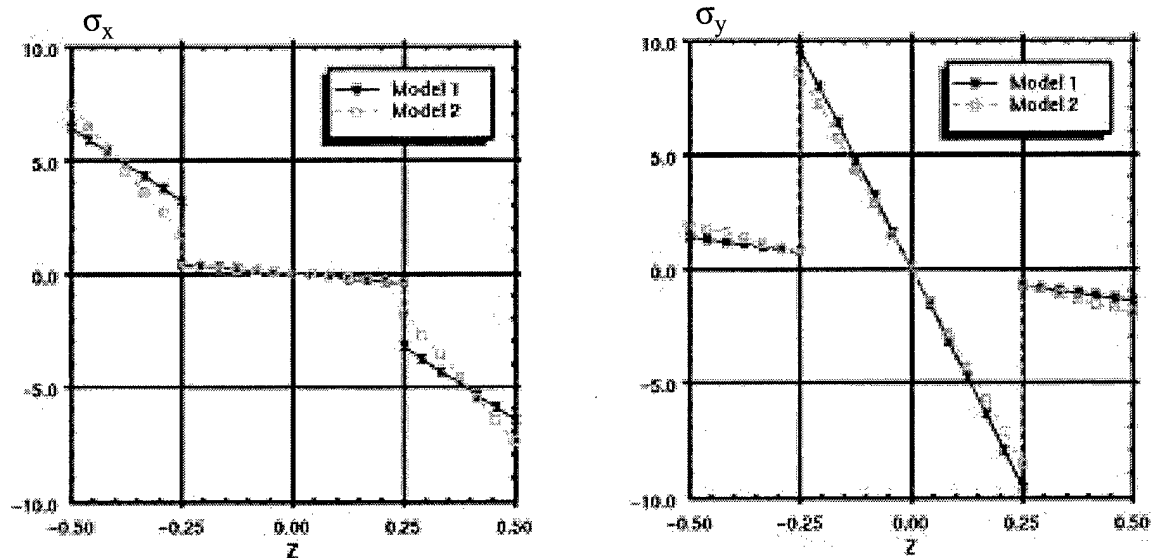
FIGURE 14. Problem 4 - Through-thickness stress distributions $\sigma_x(0,0,z)$ and $\sigma_y(0,0,z)$ for shell models 1 and 2.

faces and at the interface between layers.

3.4.2 Problem 5. Effect of boundary layers

Boundary layer effects occur at the shell boundaries, and are characterized by the fact that the solution 'near' the boundary is substantially different from the solution in the interior. All hierarchic shell models (as well as the fully three-dimensional model) exhibit boundary layers, and an important part of the energy of the solution is contained in them. For further information on boundary layer effects refer to Refs. [20] to [23]. Therefore, the mesh design necessary to obtain accurate solutions for any given member of the hierarchic sequence of models should properly account for the boundary layers. Extensive numerical experimentation clearly showed that the hierarchic models are very capable of resolving the boundary layer effects when proper meshing is used.

Based on the numerical evidence, guidelines for mesh design to be used with the hierarchic models that will provide optimal or near-optimal meshes with respect to the energy norm were developed. These guidelines are summarized as follows:

- The first step is to design a finite element mesh that provides optimal rate of convergence for the exact solution of the shell problem in the interior of the domain without consideration of the boundaries. For smooth problems and p-convergence this typically involves the use of uniform or quasi-uniform meshes. This will be referred to as the "coarse mesh".

- Once the coarse mesh is available, the boundary layers should be accounted for by the use of graded meshes. For most practical problems one or two layers of graded elements towards the edges are sufficient to account for boundary layer effects. The characteristic length of a shell problem is the thickness-to-radius ratio (h/R). For thin shells ($h/R \ll 1$), the recommended size of the boundary layer elements are $5h$ and $3\sqrt{h}$ for the first and second layers, respectively. For thick shells ($h/R \approx 1$), boundary layer effects are less significant and, in general, one layer of elements is sufficient with a size of order h.

To illustrate the effect of the boundary layer in the solution of shell problems, consider a cylinder with no kinematical constraints at the ends, subjected to a sinusoidal distributed surface traction $T_n = T_0 \cos(2\theta)$. This load is self equilibrated in the angular direction and uniform in the axial direction. The dimensions are shown in Figure 15.
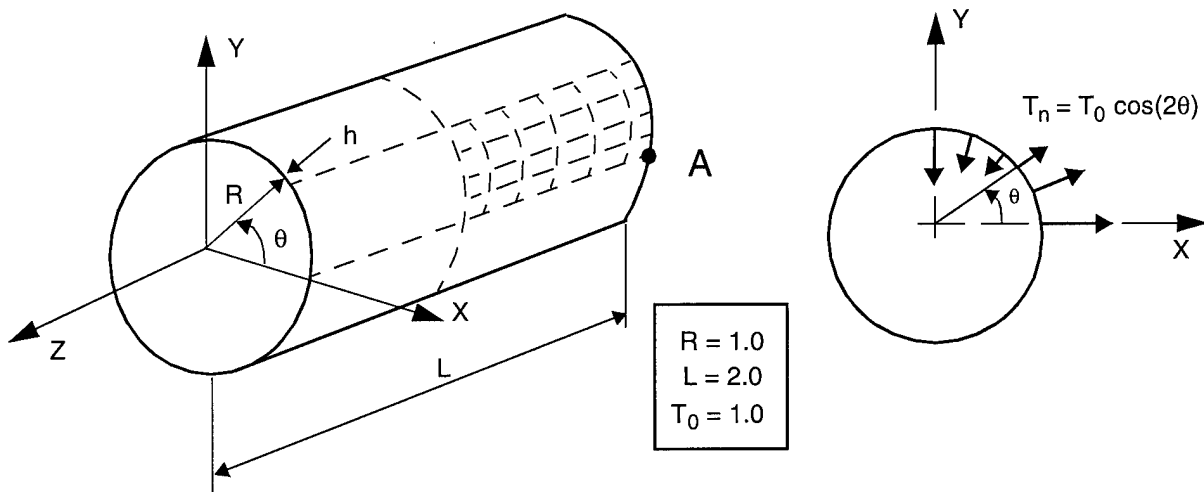
FIGURE 15. Problem 5 - Cylinder under sinusoidal loading. Notation.

Three thickness-to-radius ratios were analyzed: $h/R=0.1$, $h/R=0.01$, and $h/R =0.001$ and two different materials were considered. An isotropic material with $E=10 \times 10^6$, $v=1/3$ and unit shear factor; and a 4-ply laminated composite with a $[0/90]_s$ layup and the following properties for each layer:

$$E_L = 25 \times 10^6, \ E_T = 1 \times 10^6, \ G_{LT} = 5 \times 10^5, \ G_{TT} = 2 \times 10^5, \ v_{LT} = 0.25, \ v_{TT} = 0.49$$

where L indicates the direction parallel to the fibers and T is the transverse direction. When the L-direction coincides with the Z-direction, we refer to it as the $0°$ orientation: For the two outer layers the fibers run parallel to the Z-axis, and for the two inner layers the fibers run in the circumferential direction. All layers are of the same thickness ($h/4$). This problem is discussed in Ref. [24] for the case of isotropic material.

The radius (R=1.0) and length (L=2.0) of the cylinder are kept fixed, and the thickness is changed for each case analyzed. The solutions were obtained for hierarchic models 1 and 2, polynomial orders ranging from 1 to 8, downward run, and the product space was used. For definition of the product space, see Ref. [1], page 96.

Because of symmetry, only one sixteenth of the cylinder is considered for the analysis. Figure 16 shows the finite element mesh used for the analysis with the two boundary layer elements near the free end of the shell with sizes corresponding to h/R=0.01, that is b_1=0.05 and b_2=0.30.
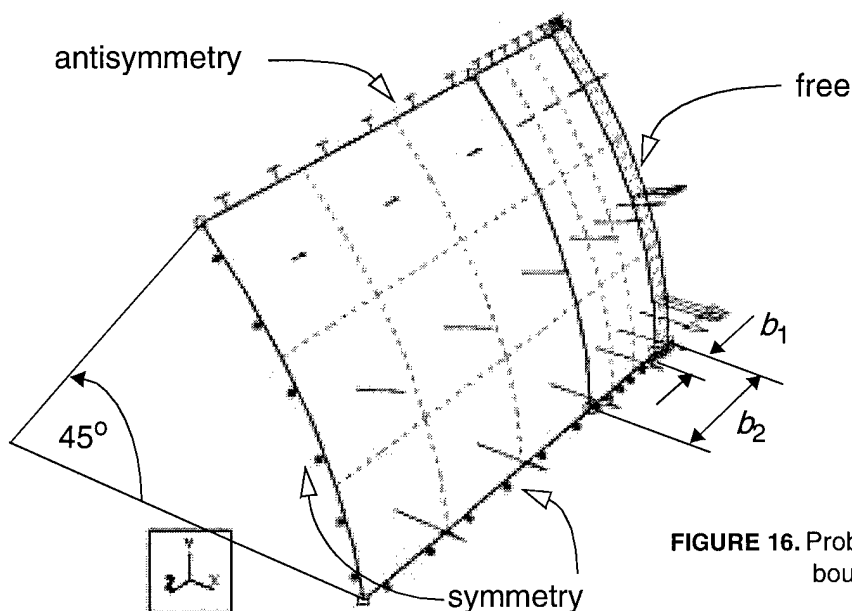
FIGURE 16. Problem 5 - Finite element mesh and boundary conditions.

The estimated relative error in energy norm as a function of the number of degrees of freedom (DOF) for each h/R is shown in Figure 17 for the case of isotropic material and in Figure 18 for the case of the 4-ply laminated composite material. All cases shown correspond to shell model 1, and the solutions converged to less than 1% relative error in energy norm. Note that the rate of convergence is very low (and consequently the error in energy norm large) for polynomial order less than 4 (run # 5) for the thick shell (h/R=0.1) and for p-levels less than 5 (run #4) for the thin shells (h/R=0.01 and 0.001). When the displacement formulation of the finite element method is used for thin shells, locking occurs when the p-level is less than 4 or 5, depending on the h/R ratio.

```
Error Estimate, ID= SOL, run #1 to #8
                                         Rate of       Estimated
Run #       DOF      Total Potential Energy  Convergence   % Error
-------------------------------------------------------------------
 8           18      -2.610236051844083e-07     0.00        99.46
 7           66      -9.361667623979584e-06     0.18        78.25
 6          144      -2.351975354867688e-05     2.03        16.10
 5          252      -2.413901861236749e-05     4.02         1.70
 4          390      -2.414594104559629e-05     6.04         0.12
 3          558      -2.414597645817654e-05     7.37         0.01
 2          756      -2.414597661870281e-05     3.55         0.00
 1          984      -2.414597663646473e-05     3.55         0.00

   Estimated Limit    -2.414597663969152e-05
```

$h/R = 0.1$

```
Error Estimate, ID= SOL, run #1 to #8
                                         Rate of       Estimated
Run #       DOF      Total Potential Energy  Convergence   % Error
-------------------------------------------------------------------
 8           18      -2.648217698062475e-06     0.00        99.99
 7           66      -1.773999616798185e-04     0.00        99.62
 6          144      -1.756527137809780e-02     0.88        50.18
 5          252      -2.330884415397600e-02     3.18         8.46
 4          390      -2.347594052532695e-02     5.83         0.66
 3          558      -2.347696117776164e-02     6.75         0.06
 2          756      -2.347696819163082e-02     3.25         0.02
 1          984      -2.347696912164808e-02     3.25         0.01

   Estimated Limit    -2.347696932677969e-02
```

$h/R = 0.01$

```
Error Estimate, ID= SOL, run #1 to #8
                                         Rate of       Estimated
Run #       DOF      Total Potential Energy  Convergence   % Error
-------------------------------------------------------------------
 8           18      -2.647732649916765e-05     0.00       100.00
 7           66      -1.790493863294442e-03     0.00       100.00
 6          144      -1.653616254975284e+01     0.79        53.98
 5          252      -2.302678201780533e+01     2.76        11.49
 4          390      -2.333055470662855e+01     4.85         1.38
 3          558      -2.333490444510118e+01     5.43         0.20
 2          756      -2.333497285630810e+01     2.31         0.10
 1          984      -2.333498856154658e+01     2.31         0.05

   Estimated Limit    -2.333499516250912e+01
```

$h/R = 0.001$

FIGURE 17. Problem 5 - Estimated relative error in energy norm. Shell model 1, **isotropic** case.

The boundary layer effects can be visualized when displaying the first principal stress distribution over the middle surface of the shell ($w = 0.0$). Even though this is a bending dominated problem, the free-edge boundary layer is present at the middle surface of the shell. Figure 19 shows the first principal stress, S_1, for the case of isotropic material and for all three thickness-to-radius ratios. Note that as the thickness of the shell decreases, S_1 is practically zero everywhere, except along a narrow band (the boundary layer) near the free edge, and that the size of the boundary layer decreases as h/R goes to zero.

```
Error Estimate, ID= SOL, run #1 to #8
                                          Rate of        Estimated
Run #        DOF         Total Potential Energy  Convergence    % Error
-----------------------------------------------------------------------
  8           18         -5.314309984125694e-07    0.00          99.61
  7           66         -1.899446773714216e-05    0.12          84.97
  6          144         -6.512955636702421e-05    1.76          21.60
  5          252         -6.828094561142016e-05    4.02           2.28
  4          390         -6.831639830084873e-05    6.31           0.15
  3          558         -6.831654203341285e-05    9.70           0.00
  2          756         -6.831654212361424e-05    1.75           0.00
  1          984         -6.831654215233987e-05    1.75           0.00
-----------------------------------------------------------------------
  Estimated Limit        -6.831654217133485e-05
```

$h/R = 0.1$

```
Error Estimate, ID= SOL, run #1 to #8
                                          Rate of        Estimated
Run #        DOF         Total Potential Energy  Convergence    % Error
-----------------------------------------------------------------------
  8           18         -5.367603163346339e-06    0.00         100.00
  7           66         -2.683182682004668e-04    0.00          99.79
  6          144         -4.745771588527027e-02    0.83          52.29
  5          252         -6.467322563428622e-02    2.97           9.94
  4          390         -6.531366484827916e-02    5.56           0.88
  3          558         -6.531869074802141e-02    8.83           0.04
  2          756         -6.531869475402023e-02    0.97           0.03
  1          984         -6.531869675536421e-02    0.97           0.02
-----------------------------------------------------------------------
  Estimated Limit        -6.531869976328750e-02
```

$h/R = 0.01$

```
Error Estimate, ID= SOL, run #1 to #8
                                          Rate of        Estimated
Run #        DOF         Total Potential Energy  Convergence    % Error
-----------------------------------------------------------------------
  8           18         -5.368169592016818e-05    0.00         100.00
  7           66         -2.695259874825106e-03    0.00         100.00
  6          144         -4.590992118544692e+01    0.78          54.48
  5          252         -6.429500566500084e+01    2.66          12.32
  4          390         -6.526508159525335e+01    4.44           1.77
  3          558         -6.528518129525122e+01    5.37           0.26
  2          756         -6.528560184167117e+01    5.28           0.05
  1          984         -6.528561843952617e+01    5.28           0.01
-----------------------------------------------------------------------
  Estimated Limit        -6.528561953032957e+01
```

$h/R = 0.001$

FIGURE 18. Problem 5 - Estimated relative error in energy norm. Shell model 1, **laminated composite** case.
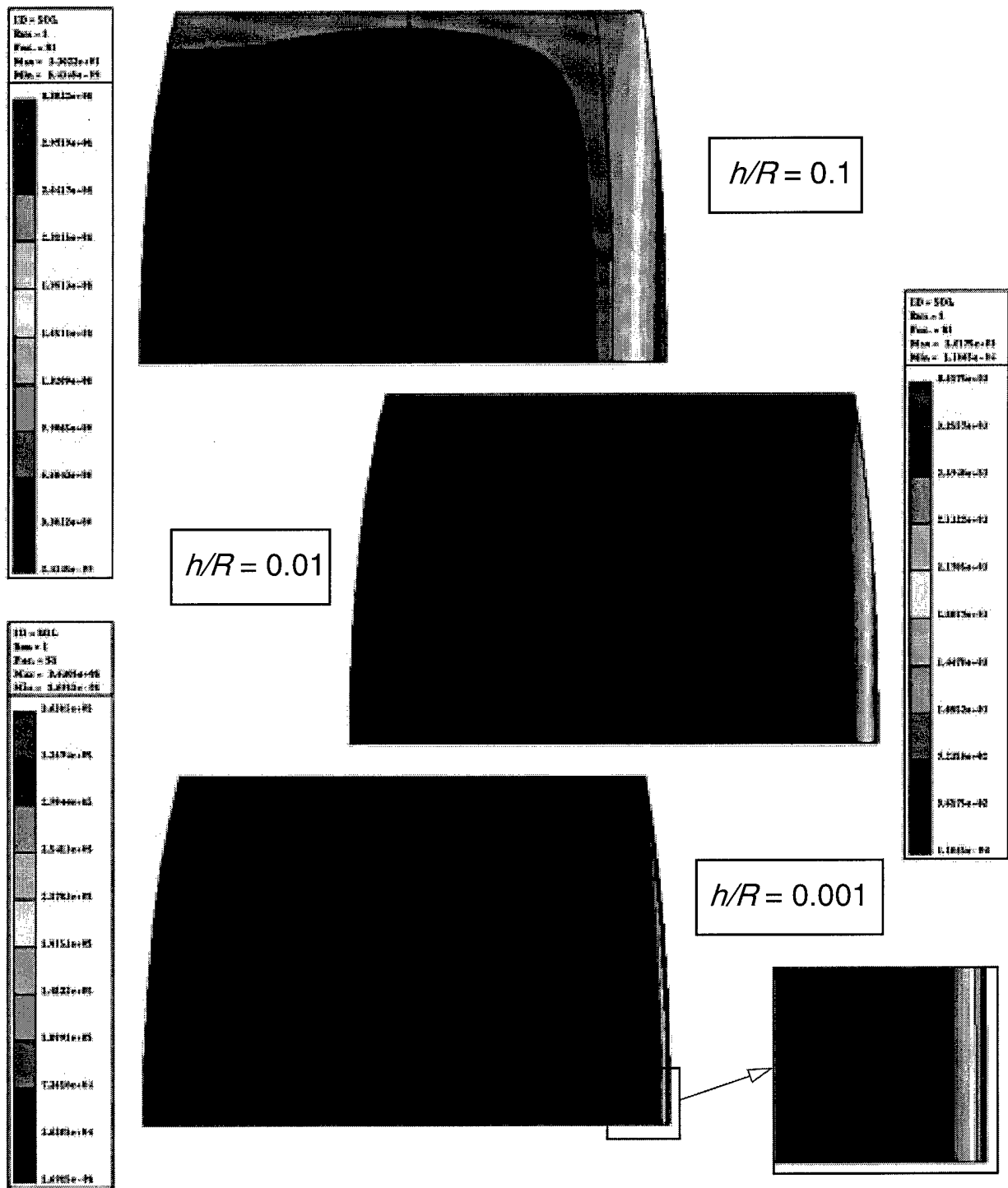
FIGURE 19. Problem 5 - First principal stress distribution at the middle surface of the shell. Shell model 1, **isotropic** case.

The boundary layer effect is also present on the external surface ($w = h/2$) of the shell. Considering the case of isotropic material shown in Figure 20, the S_1 stress distribution is rather regular every-
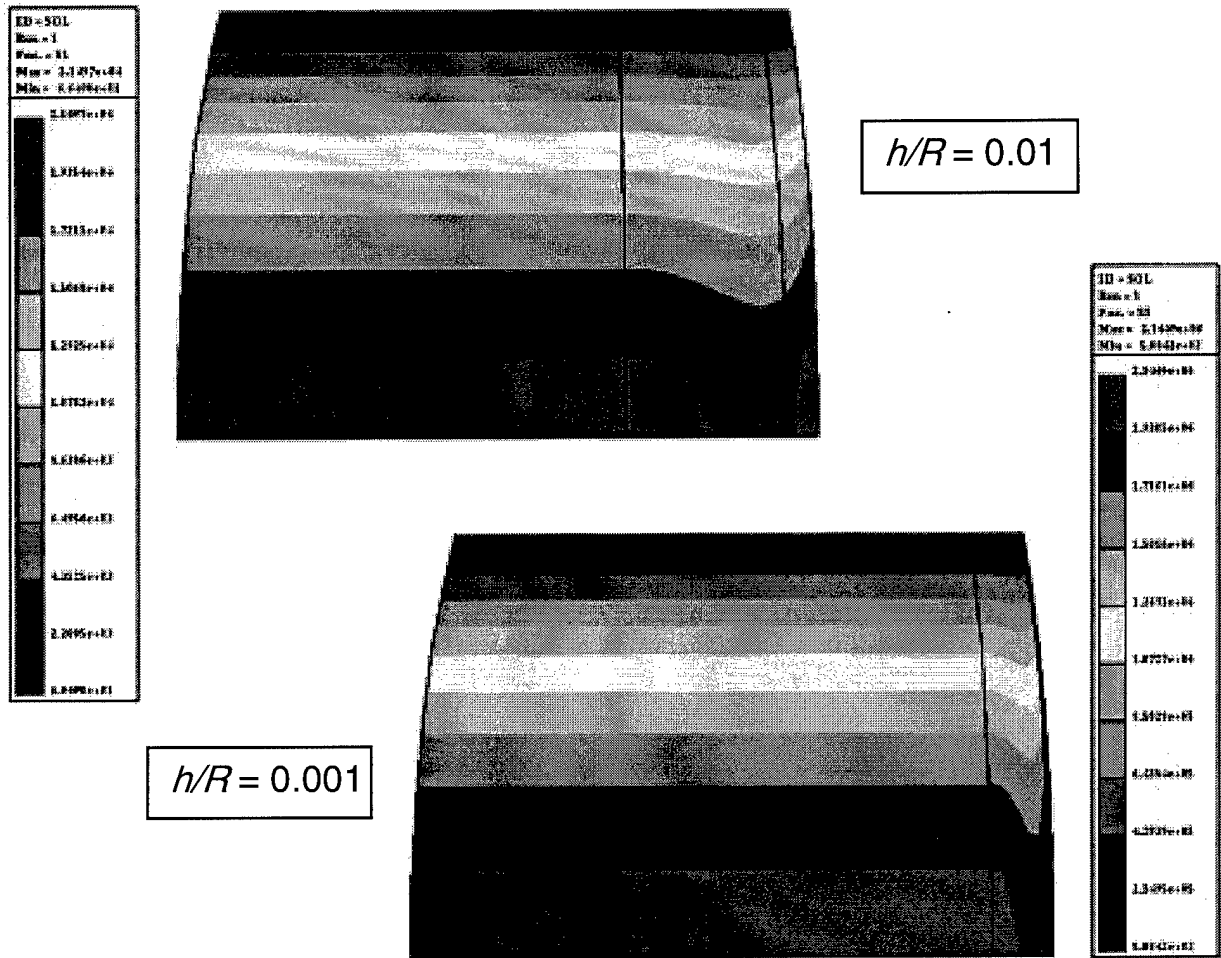

FIGURE 20. Problem 5 - First principal stress distribution at $w=h/2$. Shell model 1, **isotropic** case.

where except close to the shell free end. where the presence of the boundary layer perturb the stress distribution.

The situation is quite similar for the case of the laminated composite shell. Figure 21 shows the S_1 stress distribution for the middle surface of the shell, that is at w = 0.0, for all three h/R ratios. Comparing Figure 19 with Figure 21, the behavior of the boundary layer is almost identical for both materials.
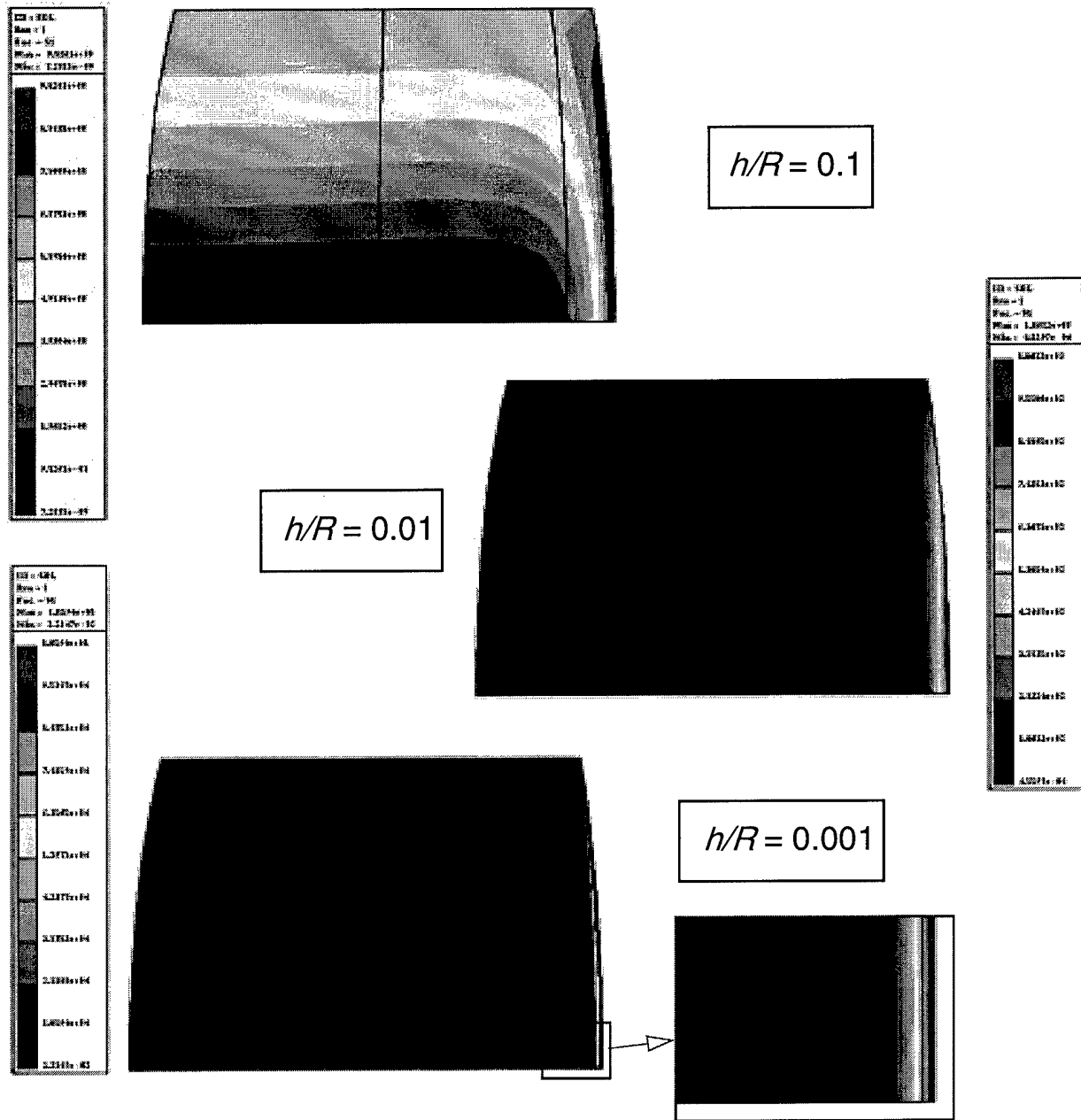
FIGURE 21. Problem 5 - First principal stress distribution at the middle surface of the shell. Shell model 1, **Laminated composite** case.

The effect of the boundary layer is less apparent at the interface between layers, however. As shown in Figure 22, the stress distribution near the free edge is only mildly perturbed by the boundary layer. The laminated composite case was also analyzed using shell model 2. No substantial difference can
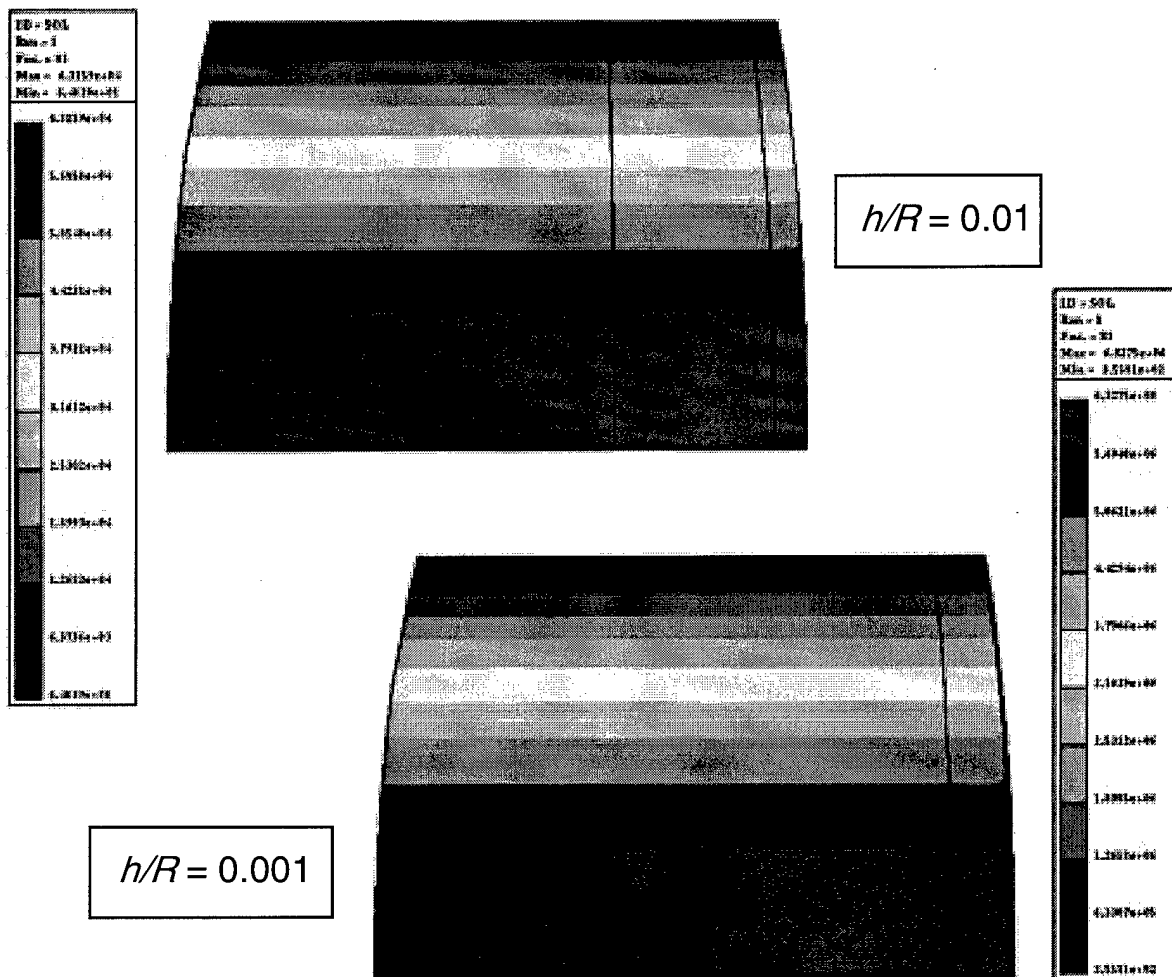
FIGURE 22. Problem 5 - First principal stress distribution at $w=h/4$. Shell model 1, **Laminated composite** case.

be realized between the results of model 1 and model 2, however. The through-thickness normal stress distribution S_y for $h/R=0.1$, at a point located at $\theta=0$ on the free end of the cylinder (point A in Figure 15), is shown in Figure 23. The results for shell models 1 and 2 are almost indistinguishable from each other. The same situation was found for the other two h/R ratios.

The first principal stress distribution, S_1, at the middle surface of the laminated composite shell is shown in Figure 24 for $h/R=0.1$ and $h/R=0.01$ as computed from shell model 2. Comparing this plot with those shown in Figure 21, it is clear that the same type of boundary layer is present in both shell models, and that the localized stresses induced are of the same order of magnitude.
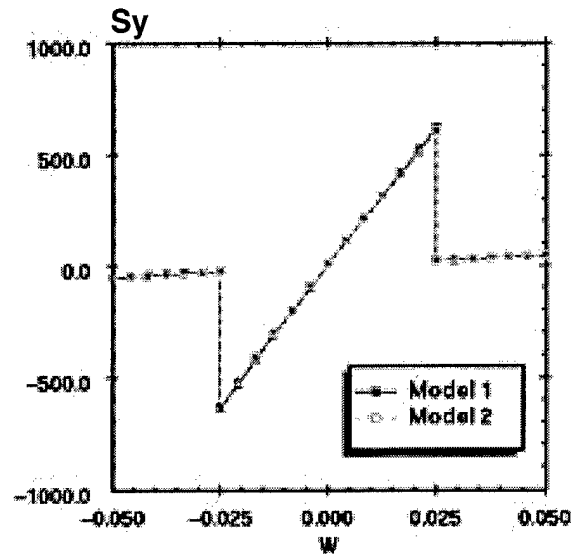
FIGURE 23. Problem 5 - Through-thickness normal stress distribution at point A. Shell models 1 and 2, **laminated composite** case.

Table 4 shows the normalized displacement of point A for all three h/R ratios and for the isotropic and laminated composite cases. The 4-ply laminate results are shown for shell models 1 and 2. The normalized displacement is defined as:

$$U = \frac{E_T h^3 u_x^A}{T_0 R^4}$$

where $E_T = 1 \times 10^6$, $T_0 = 1.0$, $R = 1.0$ and u_x^A is the displacement of point A in the global x-direction (Figure 15). Note that U converges to a limit value as the thickness-to radius ratio goes to zero, and

TABLE 4. Problem 5 - Normalized displacement of point A.

	Normalized displacement U		
h/R	**Isotropic model 1**	**Laminated model 1**	**Laminated model 2**
0.1	0.127	0.349	0.346
0.01	0.120	0.333	0.331
0.001	0.119	0.333	0.330

that both hierarchic models converge to the same value.
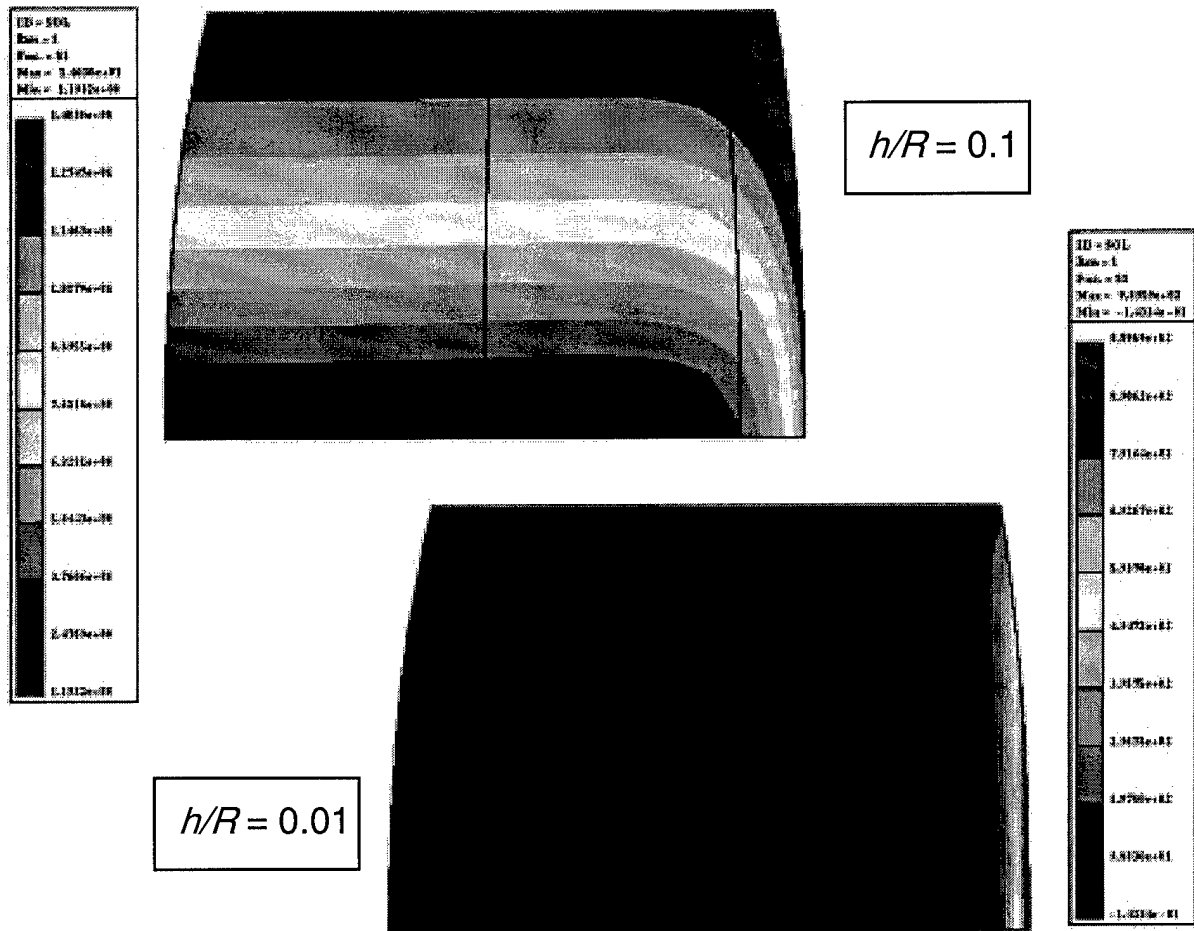
FIGURE 24. Problem 5 - First principal stress distribution at the middle surface of the shell. Shell model 2, **Laminated composite** case.

3.4.3 Problem 6. Effect of mesh distortion

The same model problem 5 is used to demonstrate the robustness of the shell models in the presence of distorted meshes. In particular, we are interested in evaluating the influence of the element edges not being aligned with the principal directions of the shell surface.

Consider the cylindrical shell shown in Figure 15 with the finite element mesh of Figure 25. The 6-element mesh was designed in such a way that the center longitudinal line can be rotated through an arbitrary angle α to change the distortion of the elements. The analysis was performed for the isotropic case and for two thickness-to-radius ratios: h/R=0.01 and h/R=0.001. Downward p extension was used together with the product space and shell model 1.
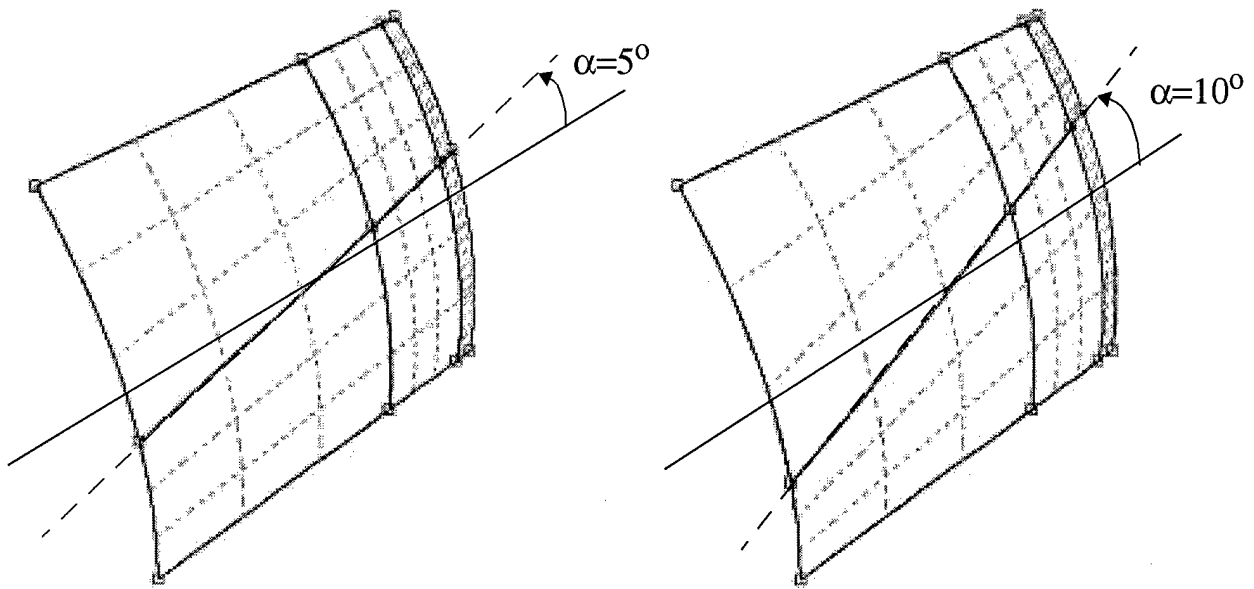
FIGURE 25. Problem 6 - Distorted finite element mesh, 6 elements

The results of the analysis are shown in Figure 26, where the estimated relative error in energy norm is shown for three values of the distortion angle α. Note that the potential energy of the solution is practically independent on the distortion angle, and for all three values of α the relative error in energy norm at p-level=8 (run #1) is very small. The results are summarized in Table 5 for both h/R ratios. Included in the table are the values of the potential energy corresponding to a p-level of 8 (run #1) and the u_x displacement component of point A (see Figure 15).

TABLE 5. Problem 6 - Effect of distortion angle, 6-element mesh

h/R	α [deg]	Potential Energy	u_x^A
	0	$-2.399350588 \times 10^{-2}$	0.122194
0.01	5	$-2.399351950 \times 10^{-2}$	0.122194
	10	$-2.399354319 \times 10^{-2}$	0.122194
	0	-23.87654257	121.602
0.001	5	-23.87655967	121.602
	10	-23.87657944	121.602

```
Error Estimate, ID= SOL, run #1 to #8
                                        Rate of        Estimated
Run #        DOF        Total Potential Energy  Convergence     % Error
-------------------------------------------------------------------------
8            36         -1.336241124934671e-05     0.00         99.97
7            132        -2.840615710935025e-03     0.05         93.89
6            288        -2.343051045818392e-02     2.32         15.32
5            504        -2.399169471407069e-02     5.13          0.87
4            780        -2.399347533110004e-02     4.67          0.11
3            1116       -2.399349983960644e-02     2.25          0.05
2            1512       -2.399350534096622e-02     3.75          0.02
1            1968       -2.399350588291860e-02     3.75          0.01
-------------------------------------------------------------------------
  Estimated Limit       -2.399350597013211e-02
```

$$\alpha = 0^o$$

```
Error Estimate, ID= SOL, run #1 to #8
                                        Rate of        Estimated
Run #        DOF        Total Potential Energy  Convergence     % Error
-------------------------------------------------------------------------
8            36         -1.289755202986731e-05     0.00         99.97
7            132        -2.654009335612438e-03     0.04         94.31
6            288        -2.328926272443428e-02     2.19         17.13
5            504        -2.399084600980942e-02     4.98          1.06
4            780        -2.399348754963635e-02     5.06          0.12
3            1116       -2.399351370342892e-02     2.36          0.05
2            1512       -2.399351895602165e-02     3.65          0.02
1            1968       -2.399351950582236e-02     3.65          0.01
-------------------------------------------------------------------------
  Estimated Limit       -2.399351960005294e-02
```

$$\alpha = 5^o$$

```
Error Estimate, ID= SOL, run #1 to #8
                                        Rate of        Estimated
Run #        DOF        Total Potential Energy  Convergence     % Error
-------------------------------------------------------------------------
8            36         -1.161274162268969e-05     0.00         99.98
7            132        -2.139050734588481e-03     0.04         95.44
6            288        -2.285085355920161e-02     1.89         21.82
5            504        -2.398729137464645e-02     4.65          1.61
4            780        -2.399350361420738e-02     5.79          0.13
3            1116       -2.399353761288973e-02     2.71          0.05
2            1512       -2.399354267072279e-02     3.65          0.02
1            1968       -2.399354319955519e-02     3.65          0.01
-------------------------------------------------------------------------
  Estimated Limit       -2.399354329008791e-02
```

$$\alpha = 10^o$$

FIGURE 26. Problem 6 - Estimated relative error in energy norm for h/R =0.01.

A second mesh design was also considered for this problem as shown in Figure 27, where a total of 10
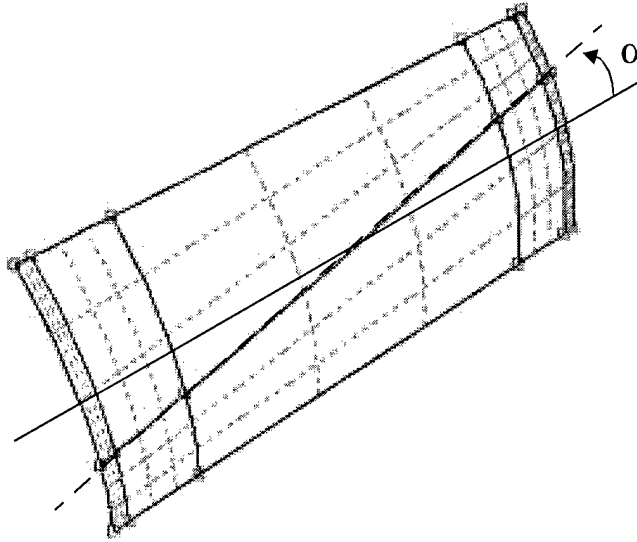

FIGURE 27. Problem 6 - Distorted finite element mesh, 10 elements.

shell elements were used. Both free ends of the cylinder are included in this mesh, and therefore boundary layer elements are required at each end.

The results for this mesh are summarized in Table 6 for h/R=0.005.

TABLE 6.   Problem 6 - Effect of distortion angle, 10-element mesh

h/R	α [deg]	Potential Energy	u_x^A
	0	-0.38308005823	0.976851
0.005	5	-0.38308003711	0.976851
	10	-0.38308000626	0.976852

All the results indicate the very low sensitivity of the solution to element distortion, even in the presence of boundary layers.

4.0 Summary and Conclusions

All objectives indicated in the Phase II proposal have been achieved.The results of the research effort were implemented in the prototype software which utilizes the data structure of Stress Check. The main accomplishments, described in detail in this report, can be summarized as follows:

- A hierarchic sequence of models for laminated composite shells was developed and implemented in the prototype software for the solution of linear elastostatics problems. These models are also capable of solving problems with isotropic or orthotropic homogeneous materials. Only three hierarchic models were implemented for laminated composites during this research Phase II. The prototype software was set up to accommodate more models once they become available in the final commercial implementation during the Phase III project.

- An automatic procedure for the selection of higher order models from the hierarchic family of models was developed and implemented in the prototype software. The automatic procedure, based on the change in the total potential energy of the problem, can be disabled so that the models can be manually selected instead.

- A unique mapping technique for shells (quasi-regional mapping) was implemented in the prototype software to handle completely general surface descriptions. The surfaces that can be created in the prototype software include spheres, cylinders, cones, torus, general surfaces created by using 3D-curves: Tabulated cylinders, extruded surfaces, ruled surfaces and surface of revolution; and surfaces created by using control points: Non-uniform rational B- and P-splines.

- The research work leading to the geometric nonlinear analysis of shells was completed in the prototype software, and the concept was implemented and tested in the 3D-solids environment. The implementation for shells will be addressed during the Phase III project. Additionally, the research and implementation of eigenvalue buckling and prestress modal analyses were completed during the Phase II project.

- The procedures for the computation of stiffness matrices, mass matrices, geometric matrices and load vectors were developed and implemented in the prototype software for quadrilateral shell elements. Similar procedures for triangular shell elements were initiated but not completed during the Phase II project. These are implementation issues, not research issues, and therefore postponed for the Phase III project.

- The following boundary conditions were implemented and tested in the prototype software for all the members of the hierarchic sequence of models:

  Loads: *Surface tractions* can be specified in global or local coordinate system or in the direction normal to the shell surface. *Edge tractions* can be specified as normal/tangent membrane, bending/twisting moments and transverse shear. *Body forces* can also be assigned in the global coordinate directions. All applied loads can be defined as constant, parametric or formula. *Point loads* can be applied to a node, point, or in the interior of the shell element either in the global or in a local reference frame. The polynomial order of the elements with points loads should be kept low (typically p=3 or 4).

Constraints: *Edge constraints* can be specified as simply support, symmetry, antisymmetry, sliding support, pinned support or built-in. *Node constraints* are allowed to prevent rigid body displacement and rotation only.

- Several representative models problems were solved using the hierarchic models, and their results compared with those available in the literature or with reference solutions obtained by solving 3D-solid models. The results clearly show the ability of the shell models to approximate the three-dimensional problem well. Many more problems than the ones included in this report were analyzed, but only a representative set was selected to illustrate the main points of the implementation.

The phase II project clearly demonstrated the potential of the use of a hierarchic sequence of models for the analysis and design of composite multilayered shells. Phase III project will address the commercial implementation of these models so that the engineering community will benefit from this new technology.

5.0 References

[1] Szabó, Barna A. and Babuska, Ivo. *Finite Element Analysis,* John Wiley and Sons, Inc. New York, 1991.

[2] Dally, James W. and Riley, Willam F. *Experimental Stress Analysis*, McGraw-Hill, Inc., 1978.

[3] Chen, Q and Babuska, I. "Approximate optimal points for polynomial interpolation of real functions in an interval and in a triangle", Comput. Methods Appl. Mech. Engrg., Vol. 128, pp. 405-417 (1995).

[4] Kiralyfalvi, G. and Szabo, Barna A. "Quasi-Regional Mapping for the p-Version of the Finite Element Method". Center for Computational Mechanics, Campus Box 1129, Washington University, St. Louis, MO 63130, December 1995. To appear in *Finite Elements in Analysis and Design,* Vol.26, Issue 1, 1998, Special issue: Robert J. Melosh medal competition.

[5] Noel, Andre T. and Szabo, Barna A. "Formulation of Geometrically Non-Linear Problems in the Spatial Reference Frame". *International Journal for Numerical Methods in Engineering*, Vol. 40, 1263-1280 (1997).

[6] Bathe, K. J. and Bolourchi, S. "Large displacement analysis of three-dimensional beam structures". *International Journal for Numerical Methods in Engineering,* Vol. 14, 961-986 (1976).

[7] Bathe, K. J. and Bolourchi, S. "A geometric and material non-linear plate and shell formulation". *Comput. Struct.*, Vol. 11, 23-48 (1980).

[8] Oliver, J. and Oñate, E. "A total Lagrangian formulation for the geometrically non-linear analysis of structures using finite elements. Part I. Two-dimensional problems: Plate and shell structures". *International Journal for Numerical Methods in Engineering*, Vol. 20, 2253-2281(1984).

[9] Liu, J. H. and Surana, K. S. "p-version axisymmetric shell elements for geometrically non-linear analysis". *Comput. Struct.*, Vol. 49, 1017-1026 (1993).

[10] Orth, F. J. and Surana, K. S. "p-version two-dimensional beam element for geometrically non-linear analysis". *Comput. Struct.*, Vol. 50, 383-392 (1994).

[11] D. Morgenster. Heldeidung der Plattentheorie aus der dreidimensionalen elastizitatstheorie. *Arch. Rational Mech.*, Vol. 42, 145-152 (1959).

[12] B. A. Szabo and G. J. Sahrmann. "Hierarchic Plate and Shell Models Based on p-Extension", *International Journal for Numerical Methods in Engineering, Vol. 26, 1855-1881 (1988).*

[13] C. Schwab. "Dimensional Reduction for Elliptic Boundary Value Problems", *Ph.D. Thesis, University of Maryland, Department of Mathematics, College Park,* 1989.

[14] Babuska, Ivo, Szabo, Barna A. and Actis, Ricardo L. "Hierarchic Models for Laminated Composites", *International Journal for Numerical Methods in Engineering, Vol. 33, 503-535.* (1992).

[15] Actis, Ricardo L. and Szabo, Barna A. 1993. "Hierarchic Models for Bidirectional Composites", *Finite Elements in Analysis and Design, Vol. 13, 149-168.*

[16] Actis, Ricardo L. "Hierarchic Models for Laminated Plates", *Ph.D. Thesis, Sever Institute of Technology, Washington University, St. Louis,* 1991.

[17] Actis, Ricardo L. "Design and analysis of laminated plates and shells". National Science Foundation, Phase I Final Report, Grant No. III-9261593, September 1993.

[18] Szabo, Barna A. and Actis, Ricardo L. "Hierarchic models for laminated plates". AMD-Vol 157, *Adaptive, Multilevel, and Hierarchical Computational Strategies*, pp. 69-94, ASME 1992.

[19] Noor, B. A., Burton, W. S. and Peters, J. M. Hierarchic adaptive modeling of structural sandwiches and multilayered composite panels. AMD-Vol 157, *Adaptive, Multilevel, and Hierarchical Computational Strategies*, pp. 47-67, ASME 1992.

[20] Arnold, D. N. and Falk, R. S. "The Boundary Layer of the Reissner-Mindlin Plate Model: Soft Simply Supported, Soft Clamped and Free Plates", *SIAM J. Math. Anal., Vol. 21, pp. 281-312* (1990).

[21] Schwab, Christoph and Wright, S. "Boundary Layer Approximation in Hierarchical Beam and Plate Models", *Department of Mathematics and Statistics, University of Maryland, Baltimore County, Baltimore, MD* 21228, USA, 1992.

[22] Schwab, Christoph and Suri, Manil. "The p and hp versions of the finite element method for problems wit boundary layers", *Department of Mathematics and Statistics, University of Maryland, Baltimore County, Baltimore, MD* 21228, USA, 1995.

[23] Gerdes, K. Matache, A. M. and Schwab, C. "Analysis of membrane locking in hp FEM for a cylindrical shell". Seminar of Applied Mathematics, Swiss Federal Institute of Technology, Zurich, Switzerland. Research Report No. 97-09, May 1997.

[24] Hakula, Harri. "High order finite element tolls for shell problems", Helsinski University of Technology, Institute of Mathematics, Research Report A376, Espoo, Finland, January 1997.